Engineering Applications of Artificial Intelligence 136 (2024) 108979

Contents lists available at ScienceDirect

Engineering Applications of Artificial Intelligence

journal homepage: www.elsevier.com/locate/engappai

Backpropagation artificial neural network-based maximum power point tracking controller with image encryption inspired solar photovoltaic array reconfiguration

Madavena Kumaraswamy *, Kanasottu Anil Naik

Department of Electrical Engineering, National Institute of Technology, Warangal, India

ARTICLE INFO

Keywords:
Artificial neural network
Bayesian regularization algorithm
Global power maximization
Levenberg-marquardt backpropagation
Maximum power point tracking

ABSTRACT

The enhancement of photovoltaic (PV) arrays through reconfiguration presents a promising avenue for increasing the global maximum power (GMP) and improving overall array performance. This enhancement is achieved by minimizing differences between rows, thereby reducing the computational load on Maximum Power Point Tracking (MPPT) systems. However, many existing reconfiguration methods face various challenges, including scalability issues, inadequate shading dispersion, distortion of array characteristics, emergence of multiple power peaks, increased mismatch, and more. In order to overcome these obstacles, this study presents a novel method for array reconfiguration that is modelled after the widely used Kolakoski Sequence Transform in picture encryption. The suggested approach is assessed in eight different scenarios with 9×9 and 5×5 PV arrays shaded differently. Its performance is compared against seven established techniques. Due to its intelligent reconfiguration aimed at minimizing shade dispersion, the suggested approach consistently outperforms alternative methods. It results in substantial improvements in GMP, enhancing it by 32.79%, 14.98%, 10.15%, and 4.13% for 9×9 arrays, and 37.10%, 14.36%, and 9.88% for 5×5 arrays across diverse conditions. Furthermore, this study comprehensively investigates three separate Artificial Neural Network algorithms, specifically the Levenberg-Marquardt (LMB), Scaled Conjugate Gradient, and Bayesian Regularization algorithms for MPPT. A Levenberg-Marquardt Backpropagation-based MPPT controller for a 250Wp standalone PV system is used to validate the effectiveness of the recommended configuration. This integrated approach, which combines reconfiguration and LMB-based MPPT utilizes only two sensors regardless of array size. It achieves accelerated convergence tracking within a short 0.13 s, displaying minimal steady-state oscillations.

1. Introduction

The drive to encourage the use of renewable energy sources arises from the desire for energy that is environmentally sustainable, free of pollutants, and in harmony with ecological principles. Because photovoltaic systems can continuously capture solar radiation, they hold the potential to provide year-round electricity to tropical countries' rural and urban areas. However, solar power generation encounters interruptions due to daily and seasonal fluctuations in sunlight exposure caused by the Earth's rotation and axial tilt (Aljafari et al., 2023). Photovoltaic panels often face partial shading (PS), a phenomenon that significantly alters their electrical properties. Shading induces variations in panel characteristics, leading to imbalances within the array and decreased efficiency (Naik et al., 2022a). In PS scenarios, shaded panels absorb energy while unshaded one's act as energy sources. This concentration of electrical current in shaded panels can create hotspots, posing potential fire hazards. Bypass protection diodes are used to redirect current during partial shading (PS) in order to lower these dangers. However, the characteristics of the array have several peaks produced by these diodes (Raj and Naik, 2023a). Multiple power peaks (MPPs) require the deployment of a maximum power point tracking (MPPT) controller in order to guarantee that the array works at the global maximum power (GMP). Nonetheless, traditional MPPT techniques can become trapped at local maxima, leading to suboptimal outcomes. Therefore, an efficient MPPT controller is essential for accurately tracking the GMP, and several recent methods have been proposed to address this challenge. An approach using an adaptive neuro-fuzzy inference system (ANFIS) to forecast the ideal duty ratio

* Corresponding author.
E-mail address: mk712052@student.nitw.ac.in (M. Kumaraswamy).

https://doi.org/10.1016/j.engappai.2024.108979
Received 20 January 2024; Received in revised form 5 June 2024; Accepted 11 July 2024
Available online 16 July 2024

has been proposed in (Ibrahim et al., 2021), allowing the tracking of the global maximum power amid many peaks. In reference (Ahmed et al., 2023), a novel approach called the adaptive perturb and observe algorithm with improved skipping feature has been introduced for rapid Global Maximum Power Point Tracking under partial shading conditions. In the cited work (Rao et al., 2023), a MPPT controller driven by a novel radial basis function neural network was designed specifically for a 7 kWp independent photovoltaic system. A distinct method employing the falcon optimization algorithm (Alshareef, 2022) is introduced to identify the Global Maximum Power Point (GMPP). The effectiveness of this approach is validated using authentic and measurable data gathered from Neom, Saudi Arabia. Although these controllers are intricate, they have limitations in maximizing the array's potential, as they primarily concentrate on Global Maximum Power (GMP) tracking. Moreover, to augment the array's output beyond what MPPT can achieve alone, array reconfiguration becomes a preferred strategy.

Improving the Global Maximum Power (GMP) and minimizing power losses in photovoltaic (PV) arrays can be effectively achieved through array reconfiguration (Raj and Naik, 2022a). These reconfiguration techniques are generally categorized as either static or dynamic, depending on how they operate. Among dynamic methods, there are three distinct approaches: Those that make use of metaheuristic algorithms, electrical array reconfiguration (EAR), and artificial intelligence (AI). In the realm of dynamic techniques, experimental validations have been conducted to evaluate the effectiveness of AI-driven reconfiguration methods. These methods employ tools such as fuzzy logic (Bouselham et al., 2021) and neural networks (Amar Raj and Naik, 2023) to mitigate losses arising from partial shading conditions (PSC). However, the implementation of these strategies demands an array of switches, sensors, and additional devices, making their execution complex. EAR-based approaches (Velasco-Quesada et al., 2009) encounter a similar challenge due to the requirement for various devices, particularly in larger PV farms. Moreover, these methods generate diverse sets of switching pulse patterns to identify the optimal one, posing a significant drawback.

In recent years, there has been a growing interest in the application of population-based metaheuristic algorithms for crafting reconfiguration switching patterns. Optimization techniques like Honey badger optimization (Chandrasekharan et al., 2023), manta ray foraging optimization (Ahmed et al., 2020), Wind driven optimization (Omer et al., 2019), Salp swarm optimization (Yang et al., 2023), Grass Hopper optimization (Mansoor et al., 2020), and Archimedes optimization (Sajid et al., 2023) have gained prominence and widespread adoption. Despite their proficiency in generating these patterns, these algorithms encounter several challenges. These challenges include extensive computational stages, time-intensive processes, difficulties in achieving convergence, managing numerous parameters, issues related to the selection of appropriate parameters and weighting factors, vulnerability to local optima, dealing with large search spaces, lengthy iterations, intricate algorithms, involvement of random elements, and the need for multi-stage problem-solving (Raj and Naik, 2022b, 2023b; Naik et al., 2022b; Rayappa David Amar Raj et al., 2023). Furthermore, while dynamic reconfiguration techniques are effective, they demand a broad spectrum of advanced components. These elements include control units, smart gadgets, switches, sensors, advanced algorithms, drive circuits that are efficient, and methodical monitoring systems. As a result of integrating these components, system complexity rises and costs do as well (Raj et al., 2020).

In light of the challenges and limitations associated with the dynamic reconfiguration strategies mentioned earlier, static reconfiguration methods have gained popularity. These methods offer a distinct advantage by eliminating the need for additional equipment, complex processes, and intricate algorithms to reconfigure arrays. Instead of relying on complicated procedures, static reconfiguration techniques encompass a variety of straightforward methods, incorporating tactics that are focused on puzzles, magic squares, shifts, indexing, analysis, logic, chaos, and patterns. Among these, puzzle-based static methods draw from structures like Sudoku (SDK) (Rani et al., 2013), Futoshiki Puzzle (FUP) (Sahu et al., 2015), Improved Sudoku (Krishna and Moger, 2019a), Optimal Sudoku (Krishna and Moger, 2019b), Hyper Sudoku (Anjum et al., 2022), Canonical Sudoku (Anjum et al., 2021), and Skyscraper Puzzle (Nihanth et al., 2019). These methods have been extensively studied using a 9×9 PV array configuration. Implementing these puzzle-based patterns aligns the PV panels to reduce current variations across rows. However, a notable drawback in all of these techniques is their lack of scalability for non-symmetrical PV array sizes. To address this limitation, the authors in (Venkateswari and Rajasekar, 2020) introduced a reconfiguration approach using a 3×3 Lo-Shu grid, similar to a magic square. This method effectively mitigated mismatch losses in the presence of partial shading. Nevertheless, the LS technique is applicable only to PV arrays of sizes $3n \times 3n$. Furthermore, magic square-based strategies (Muniyandi et al., 2023) encounter challenges when applied to arrays lacking symmetry. Due to their limited applicability, poor scalability, and susceptibility to random shade dispersion, puzzle-based and magic square-based approaches are regarded as suboptimal choices for reconfiguration.

To address shading-related issues and achieve a more balanced distribution of irradiation among different rows within an array, a scan pattern-based configuration was introduced in (Raj and Naik, 2023c). Despite its initial promise, its performance proves inconsistent under varying shading conditions, primarily due to suboptimal panel arrangement. However, this technique's effectiveness also varies when exposed to different shading scenarios. Many of these methods share a common challenge in their limited adaptability to asymmetrical PV arrays. In response to this challenge, an analytical-based technique known as odd-even (ODE) was introduced in (Nasiruddin et al., 2019), designed to be versatile for arrays of various sizes. On the basis of this framework, an improved variant known as odd-even-prime (OEP) was introduced in (Reddy and Yammani, 2020) in order to solve the shortcomings of the ODE method. Despite their scalability, the ODE and OEP are inefficient because, after reconfiguration, about half of the modules frequently stay in the same rows. Consequently, these methods typically result in efficiency improvements of less than 50%. Moreover, in specific shading scenarios, ODE and OEP schemes demonstrate subpar performance, occasionally even falling behind traditional configurations due to strong correlations between adjacent panels. Researchers in (Amar Raj and Naik, 2022) developed a method based on a two-dimensional generalized Arnold's Cat Map to address these issues. Their objective was to maximize array features under shade situations and improve the GMP.

Introducing a unique approach, the New Array Scheme (NAS), which proposes a diagonal panel arrangement (Nihanth et al., 2020) to optimize power extraction in partial shading conditions. However, the high correlation between diagonal panels compromises the effectiveness of this scheme during diagonal shading and other scenarios. In summary, while various reconfiguration techniques have been developed, they contend with issues of consistency, scalability constraints, suboptimal performance under specific shading conditions. Consequently, achieving optimal performance in PV arrays under dynamic shading remains a complex challenge. In recent times, the focus has shifted towards chaotic mapping-based strategies as a means of achieving effective array reconfiguration. Among these, the Chaotic Baker map strategy has emerged as a pioneer for reconfiguring symmetrical PV arrays (Tatabhatla et al., 2020). However, CB's efficiency remains somewhat limited, as approximately 33% of panels retain their original rows post-reconfiguration. Moreover, scaling up CB for unsymmetrical arrays is not a viable option. In response to these limitations, a novel Henon Map Transform (HMT) was introduced in (Amar Raj and Anil Naik, 2022). The HMT technique demonstrates the ability to efficiently reconfigure both symmetrical and unsymmetrical arrays. Despite its versatility, it faces challenges in dealing with cases of column shading. A new PV-TEG system combining solar and thermal energy to improve efficiency is proposed in (Yang et al., 2023). Salp Swarm Optimization

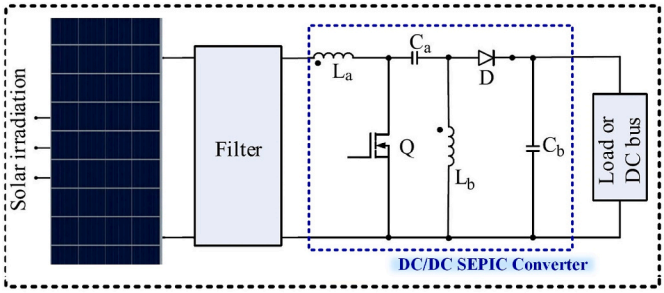

Fig. 1. Solar powered DC–DC SEPIC converter.

Table 1
Technical details of the SEPIC Converter.

Component	Specification/Rating
Inductance, L_a & L_b	1.95 mH
Capacitance, C_a	89.1 μF
Capacitance, C_b	178.05 μF
Load Resistance	159.2 Ω
Switching Frequency	5000 Hz
Output power	250Wp

tackles the challenges of shade and uneven temperatures, offering faster optimization and avoiding local maxima compared to other methods. Recently, a new method is introduced to optimize power generation from unevenly heated thermoelectric arrays (Guo et al., 2023). It divides the array into blocks requiring fewer switches and uses an improved algorithm to find the best configuration for both power output and voltage balance. The current research gaps is marked by several significant challenges, including.

- The complexity of dynamic reconfiguration processes lies in algorithms featuring weighted-sum methodologies, concerns regarding premature convergence, intricate search mechanisms, high computational demands, optimal weight determinations, challenges in parameter tuning, and the need for multi-stage solutions.
- There are several practical and financial obstacles to overcome when implementing dynamic-based algorithms since they require a large number of sensors, switches, intricate switching matrices, microcontrollers, and driver circuits.
- Most static techniques are effective solely for symmetrical array sizes, posing limitations as real-world PV arrays often have asymmetrical configurations. Choosing the best pattern from various solution sets of puzzle and logic-based strategies presents a significant challenge.
- Contemporary randomized reconfiguration strategies generate stochastic shading patterns, resulting in uneven shade dispersal, increased mismatch, variable performance, suboptimal power enhancement, reduced effectiveness in specific scenarios.
- Despite advancements in enhancing Global Maximum Power (GMP), existing strategies lead to multiple local power peaks within the array's characteristics. This imposes a significant demand on Maximum Power Point Tracking (MPPT) controllers during the pursuit of global maximum power tracking, requiring the deployment of intricate and expensive MPPT controllers.

To sum up, the research field is characterized by intricate algorithms, difficulties in implementation, constraints in adapting to asymmetrical arrays, suboptimal shading distribution, and challenges associated with local power peaks. Overcoming these hurdles is crucial for enhancing the efficiency and feasibility of PV array reconfiguration methods. In response to the limitations mentioned earlier, a highly efficient method for reconfiguring PV arrays, known as the Kolakoski Sequence Transform (KST), is introduced, utilizing integer sequences as its foundation. The innovations and contributions of this study are outlined as follows.

- This proposed Kolakoski Sequence Transform-based reconfiguration method is scalable, sensor-free, switch-free, versatile and compatible.
- Unlike many static methods (Raj et al., 2020; Rani et al., 2013; Sahu et al., 2015; Krishna and Moger, 2019a, 2019b; Anjum et al., 2021, 2022; Nihanth et al., 2019, 2020; Venkateswari and Rajasekar, 2020; Muniyandi et al., 2023; Raj and Naik, 2023c; Nasiruddin et al., 2019; Reddy and Yammani, 2020; Tatabhatla et al., 2020; Amar Raj and Anil Naik, 2022) that randomly distribute shade, the newly introduced approach employs intelligent shade dispersion. This invention reduces the correlation between neighboring modules exposed to shade in rows, columns, and diagonals by utilizing the intrinsic picture scrambling property of the selected integer sequence method. As a result, the total irradiance that particular rows within the PV array get is improved overall.
- In this study, seven previously discovered static reconfiguration strategies are thoroughly compared with the suggested KST strategy.
- Additionally, three distinct backpropagation artificial neural network algorithms, namely Levenberg-Marquardt, Scaled Conjugate Gradient, and Bayesian Regularization algorithms, have been thoroughly examined for the employment in MPPT systems.
- The viability of the proposed algorithm is further demonstrated by integrating it with a Levenberg-Marquardt Backpropagation (LMB)-based Maximum Power Point Tracking (MPPT) controller. This integration is performed within the standalone 250Wp PV system.
- Finally, the obtained MATLAB simulation results were further validated with the array's photovoltaic characteristics generated by CHROMA solar array simulator.

The remainder of the paper is organized as follows: Section II presents the mathematical modeling of the Single-Ended Primary Inductance Converter (SEPIC). In Sections III and IV, the proposed reconfiguration strategy and neural network algorithms are discussed. Section V deals with results and discussions, and the conclusions are presented in Section VI.

2. DC–DC Single Ended Primary Inductance Converter

The SEPIC (Single Ended Primary Inductance Converter) functions as a converter that doesn't invert the signal, comprising two inductors, two capacitors, a power diode, and a switch (Ding et al., 2023). It generates an output voltage with the same polarity as the input, capable of being exceeding or falling short of the input voltage to suit the load requirements. This versatile converter operates as both a buck and a boost converter, distinguished by its operational principles and design. During its active phase, when the switch is closed, current flows from the switch to one inductor (L_a) and charges another inductor (L_b) through the capacitor. When the switch is turned off, both inductors release energy, supplying current to the load-side capacitor through the diode (Fig. 1). A notable feature of this configuration is its ability to alleviate voltage stress on the capacitor by transferring energy between L_a and C_a during switching. In the 'on' interval, L_a is powered by a PV panel, while L_b is powered by C_a. Simultaneously, during the 'off' interval of the IGBT, Ca is charged by both the PV panel and L_a, while L_b discharges to either the load or the DC bus. As L_a is both charging and discharging, its current experiences linear fluctuations, resulting in a current ripple that could potentially damage the PV system, especially the MPPT (Maximum Power Point Tracking). To mitigate this issue, an input filter is introduced between the converter and the PV panel. The circuit design utilizes equations (1)–(4) to facilitate this process (Table 1). The duty cycle of the standard setup in the SEPIC converter (Guo et al., 2023) can be determined by

$$V_O = \frac{D}{1-D} V_{in} \tag{1}$$

The values for inductance, La and Lb in the converter are computed through the following

$$L_a = \frac{V_{in} D}{\Delta I_{L_a} f_s};\ L_b = \frac{V_{in} D}{\Delta I_{L_b} f_s} \tag{2}$$

To ensure the ideal inductor choice, it is advisable to maintain the ripple current at around 40% of the input current. Specifically in the context of the SEPIC converter, L_a and L_b should be equal, leading to

$$\Delta I_{L_a} = \Delta I_{L_b} = 40\%\ of\ I_{in}$$

$$\Delta V_{c_a} = 10\%\ of\ V_{in}$$

$$\Delta V_{c_b} = 10\%\ of\ V_o$$

The capacitance values of the converter are determined based on

$$C_a = \frac{I_o D}{\Delta V_{c_a} f_s};\ C_b \geq \frac{I_o D}{0.5 \Delta V_{c_b} f_s} \tag{3}$$

$$R_L = \frac{{V_O}^2}{P} \tag{4}$$

In this context, V_{in} and V_o denote the input and output voltages, ΔI_{La} and ΔI_{Lb} represent the inductor ripple currents for L_a and L_b, ΔV_{Ca} indicates the ripple voltage across C_a, ΔVc_b signifies the output ripple voltage, Iin stands for the input current, R_L denotes the load resistance, and P represents the operational power.

3. Proposed methodology

In light of the limitations observed in various reconfiguration methods outlined in prior studies, the presented reconfiguration approach adopts an intelligent approach rooted in image encryption. The methodology is elucidated as follows.

3.1. Kolakoski Sequence

The Kolakoski series is a self-referencing series in which the length of the run of succeeding symbols is described by each term (Sing, 2004). Usually, the symbols are shown as 1 and 2. The Kolakoski sequence can be expressed using an iterative formula. Let S(n) stand for the sequence's n-th term.

1. For $n = 1$, S (1) = 1.
2. For $n = 2$, S (2) = 2.
3. For $n > 2$, the value of S(n) depends on the value of S($n-1$) & the length of previous run:
   - If S($n-1$) = 1, then S(n) = 2.
   - If S($n-1$) = 2, then S(n) = 1.
   - The length of the run is determined by the value of S($n-1$).

Here is a recursive representation of the Kolakoski sequence using the above rules:

$$S(n) = \begin{cases} 1 & if\ n = 1 \\ 2 & if\ n = 2 \\ S(n) = 2 & if\ S(n-1) = 1 \\ S(n) = 1 & if\ S(n-1) = 2 \end{cases} \tag{5}$$

This recursive representation provides a way to compute the values of the Kolakoski sequence terms sequentially.

Algorithm 1. Generation of Kolakoski Sequence
Input: Desired sequence length (length)
Output: Kolakoski sequence (S)

1. Initialize Kolakoski sequence S with [1, 2] (first two terms).
2. Set current_index = 2 (index of the last term in S).
3. While length of S < length:
4. Determine the next run length based on S[current_index]:
5. If S[current_index] = = 1:
6. Add 2 to S for the next two terms (S.append(2), S.append(2)).
7. Else:
8. Add 1 to S for the next one term (S.append(1)).
9. Update current_index + = 1.
10 Return the Kolakoski sequence S.

End Algorithm.

The pseudocode in Algorithm.1 outlines the basic steps in generating the Kolakoski series. The sequence starts with 1.The first element is 1, so the next run is 2 (one 2).now, the sequence is 1, 2.the second element is 2, so the next run is 2, 2 (two 2s).now, the sequence is 1, 2, 2.the third element is 2, so the next run is 1, 1 (two 1s).now, the sequence is 1, 2, 2, 1, 1.the fourth element is 1, so the next run is 2 (one 2).now, the sequence is 1, 2, 2, 1, 1, 2.the fifth element is 1, so the next run is 2 (one 1).continue this process …

Algorithm 2. Pseudocode of the proposed KST_Encryption:
Input: Initial matrix 'G' characterized by its dimensions (rows, columns, 2).
Output: Resultant encrypted matrix 'H'.

1. Determine the dimensions of the input matrix 'G' as **[rows, columns] .**
2. Initialize the **iteration counter** to 0.
3. Set the **termination criteria** for the loop.
4. **While** the iteration counter is less than the termination criteria:
5. Identify the largest symmetrical sub-matrix starting from coordinates (0, 0).
6. **For** each row from 1 to the total number of rows:
7. **For** each column from 1 to the total number of columns:
8. Record the current positions as old_coordinates.
9. Calculate new_coordinates using the KST_Transform function, taking the modulus of [rows, columns].
10. Swap the pixel values: H (i, j) ← G(new_coordinates [1], new_coordinates [2].
11. **End for**
12. **End for**
13. Apply the process to all symmetrical sub-matrices.
14. Increment the iteration counter by 1.
15. **End while**

End Algorithm.

3.2. Kolakoski Sequence Transform

The Kolakoski sequence (Sing, 2004) initiates with the sequence: 1, 2, 2, 1, 1, 2, 1, 2, 2, 1, 1, 2, 1, 2, 2, 1,1,2 …… Various encryption transformations can be created by combining these terms. The Kolakoski sequence-Transform (KST) is defined through the mapping KS: $T^2 \rightarrow T^2$.

$$\begin{bmatrix} x(i+1) \\ y(i+1) \end{bmatrix} = \begin{bmatrix} K_i & K_{i+1} \\ K_{i+2} & K_{i+3} \end{bmatrix} \begin{bmatrix} x(i) \\ y(i) \end{bmatrix} \bmod N \tag{6}$$

The digital image has a dimension of N, where x and y take values from the set {0, 1, 2, …, N-1}. Here, Ki represents the ith term of the Kolakoski series, where i ranges from 1 onwards. By assigning $\begin{pmatrix} K_i & K_{i+1} \\ K_{i+2} & K_{i+3} \end{pmatrix}$ as KST_i within this series, the initial matrix is specified as:

$$KST_1 = \begin{pmatrix} K_1 & K_2 \\ K_3 & K_4 \end{pmatrix} = \begin{pmatrix} 1 & 2 \\ 2 & 1 \end{pmatrix}$$

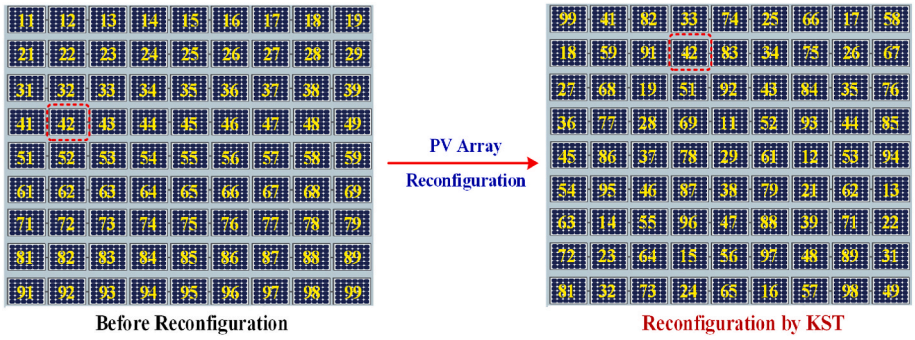

Fig. 2. Pixel scrambling using proposed KST for a 5 × 5 array Before Reconfiguration and After Reconfiguration.

Table 2
Parameters of neural networks.

Learning Rate	0.001
Number of Epochs	1000
Layer size	10
Number of hidden layer	1
Activation Functions	Sigmoid Activation Function
Optimizer	Gradient Descent
Dropout Rate	0.1
Regularization Parameters	0.01

By proceeding in this fashion, an infinite number of transformations can be generated. Here are the expressions for the second and third transformation matrices in the KST sequence

$$KST_2 = \begin{bmatrix} K_2 & K_3 \\ K_4 & K_5 \end{bmatrix} = \begin{bmatrix} 2 & 2 \\ 1 & 1 \end{bmatrix}, KST_3 = \begin{bmatrix} K_3 & K_4 \\ K_5 & K_6 \end{bmatrix} = \begin{bmatrix} 2 & 1 \\ 1 & 2 \end{bmatrix}, \quad (7)$$

The sequence can also yield a wide variety of transformation matrices by altering the value of 'i.' Algorithm 1 gives the pseudocode for KST scrambling. Moreover, an additional scrambling effect is produced by continually employing Eq. (8) in the subsequent procedure.

$$\begin{bmatrix} x(i+1) \\ y(i+1) \end{bmatrix} = \begin{bmatrix} K_i & K_{i+1} \\ K_{i+2} & K_{i+3} \end{bmatrix}^n \begin{bmatrix} x(i) \\ y(i) \end{bmatrix} \bmod N, n \geq 2 \quad (8)$$

3.3. PV array reconfiguration using KST methodology

The encryption process entails modifying the image using a 2 × 2 transformation matrix derived from consecutive terms within the Kolakoski Sequence Transform, applied to individual pixels. This is exemplified in Fig. 2, where pixel 42 from the original 9 × 9 matrix, positioned at coordinates (4, 2), is shifted to coordinates (2, 4) through KST application. This method shuffles matrix pixels (representing the image) to minimize correlations between neighboring pixels. To illustrate, a photovoltaic (PV) array comprises interconnected solar panels organized in parallel and series, akin to how pixels form an image (as depicted in Fig. 2). Here, each solar panel corresponds to an image pixel, and the entire PV array is analogous to a composite image. This analogy facilitates KST encryption. Aligning array panel configurations based on modified KST matrix patterns evenly disperses shading across the PV array. This arrangement optimizes shadow distribution and mitigates row current disparities. Panels are strategically interconnected using KST-derived patterns, preserving electrical circuitry integrity. This method counteracts shading effects uniformly, preventing multiple power peaks and preserving array characteristics. Fig. 2 shows the initial array configuration. For instance, panel number "36″ is located in the third row and sixth column. After applying the reconfiguration strategy based on encrypted matrices, panel "36″ is now in the fourth row and first column. This demonstrates how the strategy effectively repositions all panels to distribute shading uniformly. For instance, if the panels PV99, PV41, PV82, PV33, ….,PV58 (originally in the first row) become shaded in the reconfigured array, the impact is spread across all rows electrically. This balances irradiation and mitigates mismatch.

4. Global power tracking of PV system

The methods used to track the maximum power point are examined in this part, including the traditional perturb and observe (P&O) method (Raiker and Loganathan, 2021) for MPPT and MPPT controllers that make use of several types of backpropagation neural networks.

4.1. Backpropagation ANN learning-based MPPT controllers for PV system

In this section, three distinct artificial neural network algorithms namely Levenberg-Marquardt (de Jesús Rubio, 2020), Scaled Conjugate Gradient (Khadse et al., 2016), and Bayesian Regularization (Sharma et al., 2023) algorithms (Fig. 6) have been tested to validated to employ the best one for the proposed reconfigured PV system. Additionally, the selected MPPT control strategy anticipates the perfect duty ratio that matches the voltage and current output of the generated array.

4.2. Data collection and neural network training process

To acquire the training and testing datasets, a MATLAB Simulink model of the PV system, operating without MPPT controller, is constructed. This model undergoes rigorous testing in various uniform and non-uniform shading scenarios, accurately recording the optimal duty ratio values corresponding to current and voltage of array under each shading condition. Following this procedure, 31 sets of data comprising the three electrical parameters have been obtained. The gathered dataset is subsequently employed to train and test the NN model. To initiate the training of a neural network, input 'nnstart' in the command window and launch the application tailored for this purpose. Choose the input-output fitting option, which will reveal a two-layer feedforward network on the display. Then, import the required data from the workspace and specify the data for network training. Navigate through the saved workspace data to identify suitable input and output parameters. The training process concludes once this step is finished and the following methods are employed for training.

- Train using the Levenberg-Marquardt backpropagation algorithm
- Train with Bayesian regularization backpropagation
- Train using the scaled conjugate gradient method

Subsequently, proceed to export the model by transferring the developed neural network block to the MATLAB Simulink environment. This process results in the creation of a function-fitting network. Thirty percent of the dataset is divided equally between testing and validation, with the remaining seventy percent going toward training. The considered neural network has one hidden layer. This hidden layer utilizes a

Table 3
Levenberg-marquardt training parameters and criteria.

Unit	Initial value	Stopped value	Target value
Epoch	0	**11**	**1000**
Elapsed Time	–	00:00:00	–
Performance	0.0997	2.5e-05	0
Gradient	0.127	4.46e-05	1e-07
Mu	0.001	1e-05	1e+10
Validation Checks	0	6	6

Table 4
LMB-NN performance on Training, Validation, and Test Data.

	Observations	MSE	R
Training	21	7.5001e-05	0.9933
Validation	5	2.4475e-04	0.9802
Test	5	6.0356e-04	0.9736

sigmoid transfer function to activate its neurons. The Layer size is considered as 10, defining the number of neurons within this hidden layer. The input layer has two neurons, corresponding to the two features present in the data (Table 2). Similarly, the output layer likely consists of a single neuron. Finally, the output layer employs a linear transfer function, and the LMB, BR, and SCG backpropagation algorithms are used to train the model. The Comparison of the LMB, SCG, BR in terms of various parameters is as shown in Table 9.

4.2.1. Levenberg-Marquardt Backpropagation

Levenberg-Marquardt Backpropagation (LMB) (de Jesús Rubio, 2020) resolves nonlinear optimization challenges efficiently. It functions as a second-order training algorithm for loss functions represented as sums of squared errors, similar to Quasi-Newton methods but without the need for computing the exact Hessian matrix. It computes both the gradient vector and the Jacobian matrix. Below is a detailed step-by-step explanation of the provided LMB pseudocode.

Step 1- Initialize Weights(w) and Biases(b): Start with small random values for network parameters, ensuring proper initialization for effective optimization.
Step 2- Set Hyperparameters: Define damping factor (λ) for LMB updates, maximum iterations, and target loss to guide convergence.
Step 3- Training Loop: Iterate through max_ iterations for training processes.
Step 4-Forward Propagation: Calculate weighted inputs, apply activation function for predictions, using current weights and biases.

$$\text{Weighted input calculations} : z = w * x + b \tag{9}$$

Activation function applications: a = activation(z)

Step 5- Compute Loss and Gradients: Evaluate error using a loss function, and determine partial derivatives with respect to weights (Jacobian matrix).

$$\text{Loss calculation} : L = \sum_i (t_i - a_i)^2 \tag{10}$$

Gradient vector calculations: ∇L.
't' represents the target output, a represents the predicted output.

Step 6- Compute LMB Update: Formulate matrices for LMB update equation, solve resulting linear system.

$$\text{Jacobian matrix calculation} : J = \frac{\partial a}{\partial w} \text{ (partial derivatives w.r.t to weights)} \tag{11}$$

$$\text{The Levenberg} - \text{Marquardt update equation} : = \left(J^T * J + \lambda * I\right) * \Delta w = J^T * \nabla L \tag{12}$$

Step 7- Update Weights and Biases: Adjust weights with LMB update (excluding bias) and modify biases.

$$\text{Update Weights} : w = w + \Delta w \tag{13}$$

$$\text{Update Biases } b = b + \Delta b \text{ where} \Delta \text{b is the last element of} \Delta \text{w} \tag{14}$$

Step 8- Calculate New Loss: Recalculate error using updated weights and biases for revised loss.
Step 9- Check Convergence: Verify if $|L_{new} - L_{old}| <$ target loss. If true, optimization converges, exit loop.
Step 10- Adjust Damping Factor: Modify λ based on error change, enlarging or diminishing step size.
Step 11- Print Progress: Optionally, log current iteration and new error for monitoring.
Step 12- Terminate and Evaluate: Conclude training if error change < target or max_iterations reached. Evaluate model performance using independent dataset.

During the Levenberg-Marquardt Training process, several parameters, including epochs, elapsed time, performance (error), gradient, and the adaptive parameter Mu, are meticulously recorded at different stages of training. Initially, the model exhibits a performance of 0.0997, which remarkably improves to 2.5e-05 by Epoch 11 and eventually reaches the desired target of 0 by Epoch 1000, indicating a highly successful training process (Table 3). The gradient values steadily decrease, indicating convergence, while the adaptive parameter Mu undergoes significant adjustments throughout the training, showcasing the algorithm's adaptability. Furthermore, validation checks are conducted six times at both Epoch 11 and 1000 to ensure the model's consistency. At Epoch 11, the model demonstrates an outstanding fit with a mean squared error (MSE) of 7.5001e-05 on the training dataset, coupled with a high correlation coefficient (R) of 0.9933 (Table 4). This high R value suggests a robust positive correlation between predicted and actual values. Although the MSE is slightly higher on the validation dataset (2.4475e-04), the model displays strong and consistent performance, indicating its ability to generalize effectively to unseen data (Fig. 3).

4.2.2. Bayesian Regularization

Bayesian Regularization (Sharma et al., 2023) transforms nonlinear regression into a statistical problem and enhances neural network training resilience compared to standard backpropagation. It reduces the need for extensive cross-validation. Here's a systematic guide for applying Bayesian regularization in neural network training through backpropagation.

Step 1- Initialize Weights and Biases: Set neural network weights (w) and biases (b) to small random values, crucial for preventing gradient issues.
Step 2- Set Hyperparameters: Choose learning rate, η (small positive value) and regularization parameter (λ) to control regularization.
Step 3- Training Loop: Iterate for a fixed number of epochs over the dataset.
Step 4- Forward Propagation: Compute weighted sum of inputs, apply activation function for anticipated output.

$$\text{weighted sum of inputs calculations} : z = w * x + b \tag{15}$$

activation function application: $a = activation(z)$.

Step 5- Compute Loss: Contrast predicted output with actual labels using suitable loss function (mean squared error, cross-entropy).

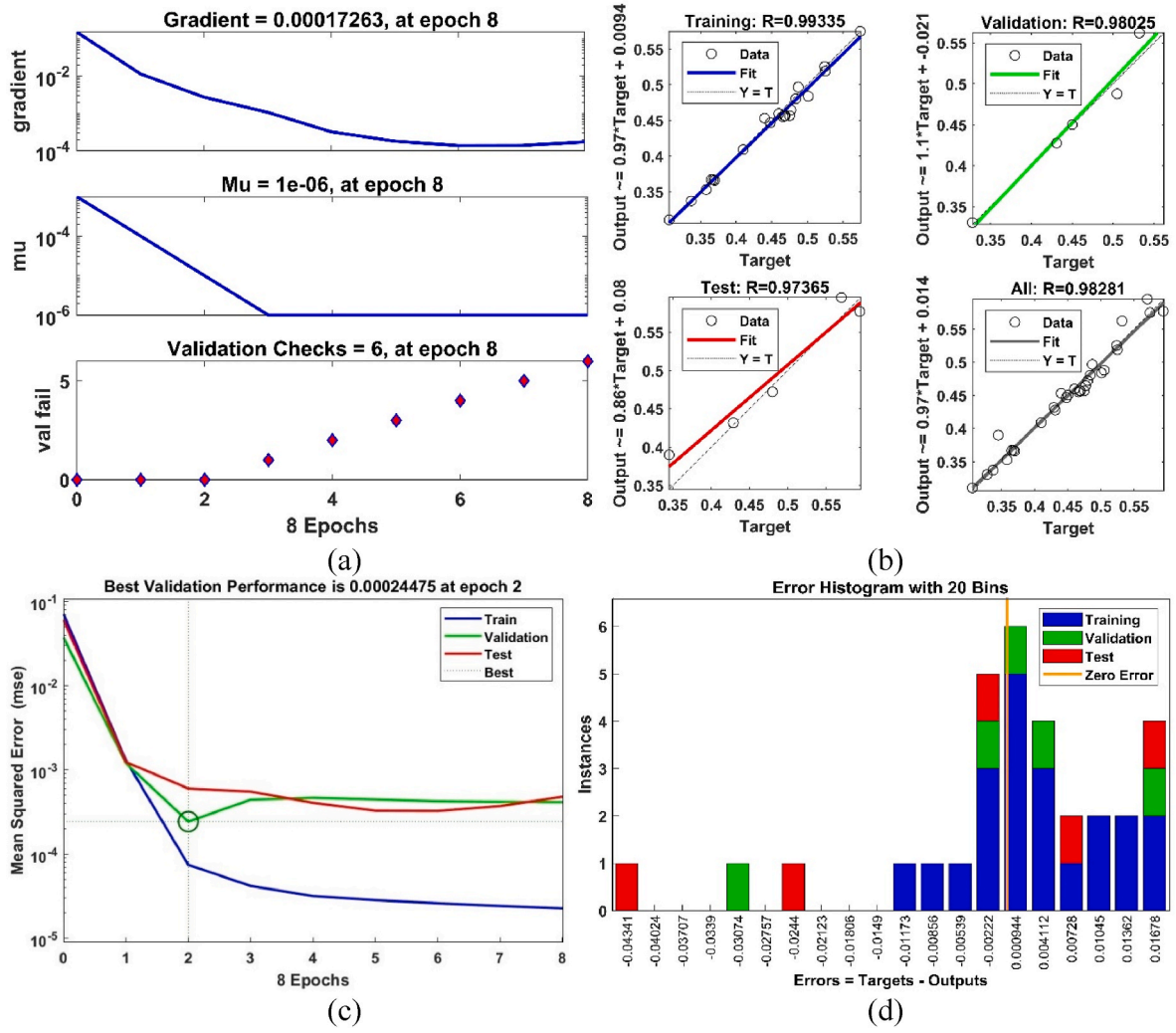

Fig. 3. (a) Training state plot, (b) regression plot, (c) performance plot, (d) error histogram plots obtained by LMB-NN.

Table 5
Bayesian regularization training parameters and criteria.

unit	Initial value	Stopped value	Target value
Epoch	0	179	1000
Elapsed Time	–	00:00:00	–
Performance	0.111	3.97e-05	0
Gradient	0.212	1.82e-05	1e-07
Mu	0.005	5e+10	1e+10
Effective # Parameters	41	8.7	0

$$\text{Mean Squared Error Loss} : L = \frac{1}{N}\sum_{i=1}^{n}(t_i - a_i)^2 \tag{16}$$

$$\text{Cross Entropy Loss} : L = -\frac{1}{N}\sum_{i=1}^{n}(t_i * \log(a_i) + (1 - t_i) * log(1 - a_i)) \tag{17}$$

Here 't' represents the target output, 'a' represents predicted output, and 'N' is the number of samples.

Step 6- Compute Regularization Gradient: Determine gradient of regularization term, λ times weights for regularization.

$$\text{Gradient of regularization term} : \frac{\partial}{\partial w}(\lambda * \|w\|)^2 = 2 * \lambda * w \tag{18}$$

Step 7- Compute Total Gradient: Calculate gradient of loss function with respect to weights using chain rule.

$$\text{gradient of total loss function} : \nabla L = \frac{\partial L}{\partial a} * \frac{\partial a}{\partial z} * \frac{\partial z}{\partial w} + 2 * \lambda * w \tag{19}$$

Step 8- Update Weights and Biases: Adjust weights and biases by subtracting scaled gradients, considering learning rate.

$$\text{Updated Weight} : w = w - \eta * \nabla L \tag{20}$$

$$\text{Updated Biase} : b = b - \eta * \frac{\partial L}{\partial z} \tag{21}$$

Step 9- Repeat: Iterate through steps 4–8 for specified epochs.
Step 10- Evaluation and Fine-Tuning: Evaluate model using separate dataset. Refine hyperparameters based on validation results,

Table 6
BR-NN performance on Training and Test Data.

	Observations	MSE	R
Training	26	3.9725e-05	0.9963
Test	5	3.3350e-04	0.9683

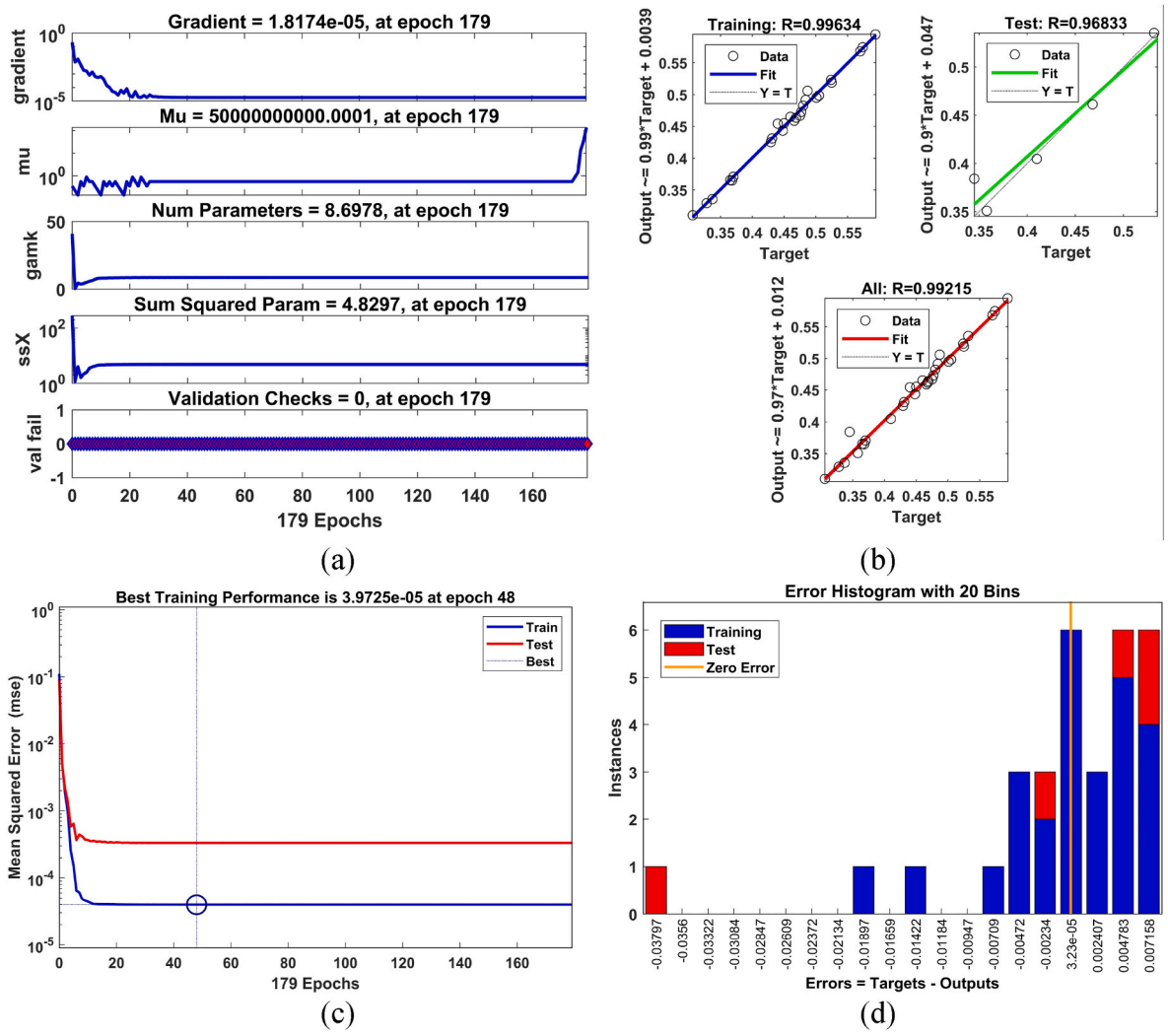

Fig. 4. (a) Training state plot, (b) regression plot, (c) performance plot, (d) error histogram plots by BR-NN.

Table 7
Scaled conjugate gradient training parameters and criteria.

unit	Initial value	Stopped value	Target value
Epoch	0	30	1000
Elapsed Time	–	00:00:00	–
Performance	0.134	7.06e-05	0
Gradient	0.223	0.000553	1e-06
Validation Checks	0	6	6

Table 8
SCG-NN performance on Training, Validation, and Test Data.

	Observations	MSE	R
Training	21	8.3030e-05	0.9925
Validation	5	1.1579e-04	0.9947
Test	5	8.3171e-05	0.9972

including learning rate, regularization, and epochs, to enhance efficacy.

Table .5 presents a comprehensive summary of the neural network training process incorporating Bayesian Regularization. This approach involves monitoring initial, stopped, and target values for various parameters across epochs, reflecting the training progression. Initially, the model's performance, evaluated using an error metric, stands at 0.111 but significantly improves to 3.97e-05 by Epoch 179, eventually reaching the target of 0 by Epoch 1000. The gradient, representing the error surface's rate of change, decreases from 0.212 to 1.82e-05, indicating the model's convergence. The parameter "Mu," vital in the Bayesian Regularization algorithm, notably increases from 0.005 to 1e+10, showcasing adaptive adjustments during training. Model complexity is effectively reduced, as evidenced by the decrease in the effective number of parameters from 41 to 8.7 due to regularization. The training dataset displays a minimal mean squared error (3.9725e-05) and a strong correlation coefficient (0.9963) (Table 6). Similarly, the test dataset exhibits a relatively low mean squared error (3.3350e-04) and a robust correlation coefficient (0.9683), demonstrating the model's ability to generalize to new, unseen data (Fig. 4).

4.2.3. Scaled conjugate gradient

The Scaled Conjugate Gradient (SCG) method (Khadse et al., 2016) aims to streamline the line search process by exploring conjugate directions, which typically lead to faster convergence than traditional methods. It requires derivative functions for weights, net inputs, and transfer functions in neural network training. SCG bridges between gradient descent and Newton's method, eliminating the need for evaluating, storing, and inverting the Hessian matrix required by Newton's technique. It was designed to accelerate the convergence of gradient descent.

Step 1- Initialize Weights and Biases: Set initial values for weights and biases randomly to avoid gradient-related issues.
Step 2- Set Hyperparameters: Define key parameters like max_iterations, target_loss, and epsilon.
Step 3- Training Loop: Iterate for a specified number of times (max_iterations) to train the neural network.
Step 4- Forward Propagation: Use existing weights and biases to predict output based on input data.

$$\text{weighted sum of inputs calculations} : z = w * x + b \tag{22}$$

activation function application: $a = activation(z)$.

Step 5- Compute Loss and Gradients: Assess error using a suitable loss function. Calculate gradients to understand the rate of error change concerning weights and biases.

Loss calculation: L = Loss (t, a) where t is the target output, a is the predicted output

$$\text{Gradient vector calculation} : \nabla L = \frac{\partial L}{\partial w} \tag{23}$$

Step 6- Compute Jacobian Matrix: Determine partial derivatives of network output with respect to weights, providing insight into weight impact on predictions.

$$\text{Partial derivatives of network output with respect to weights} : J = \frac{\partial A}{\partial w} \tag{24}$$

Step 7- Compute Hessian Diagonal: Calculate diagonal of the Hessian matrix using Jacobian information, crucial for effective optimization.

$$\text{Diagonal elements of the Hessian matrix} : H_d = \frac{\partial^2 L}{\partial w^2} \tag{25}$$

Step 8- Compute Scaled Gradient and Hessian: Scale gradients using square root of the Hessian diagonal. Scaled hessian integrates Jacobian and Hessian data, guiding accurate weight adjustments.

$$\text{Scaled gradient} : = \frac{\nabla L}{\sqrt{H_d + e}} \tag{26}$$

$$\text{Scaled Hessian} : = \frac{J}{\sqrt{H_d + e}} \tag{27}$$

Step 9- Compute Search Direction: Solve linear equations involving scaled Hessian and scaled gradient to find optimal weight adjustments, minimizing error.

$$Scaled\ hessian \times Search\ direction = Scaled\_gradient \tag{28}$$

Step 10- Line Search for Step Size: Implement line search algorithm to find step size minimizing error along the search direction.
Step 11- Update Weights and Biases: Adjust weights by moving in the calculated search direction, ensuring convergence toward optimal solution.

$$\text{Updated weight} : w = w + step\_size \times \text{search}\_direction \tag{29}$$

Step 12- Compute New Loss: Reevaluate error using updated weights and biases to assess model performance after adjustments.

Reevaluate error using updated weights and biases: L_{new} = loss (t, a_{new})

Step 13- Check Convergence: Verify if absolute error change is less than the target loss, indicating successful optimization and convergence.

Verify,

$$if |L_{new} - L| < target_{loss} \tag{30}$$

Step 14- Termination and Evaluation: Conclude training loop and evaluate model's predictive effectiveness using validation or test data.

In Table 7 the Scaled Conjugate Gradient methodology, crucial parameters such as epochs, performance metrics, gradient values, and the number of validation checks are outlined. The training initiates at Epoch

Table 9
Comparison of the LMB, SCG, BR in terms of various parameters.

Advantages	Levenberg-Marquardt backpropagation (LMB)	Scaled Conjugate Gradient (SCG)	Bayesian Regularization (BR)
Convergence Speed	Rapid, especially for well-conditioned problems and close guesses.	Quick, though can be slower in specific cases.	Generally slower due to probabilistic nature and iterative updates.
Adaptability to Problem	Adapts well to local error surface geometry.	Adaptable, although struggles with poor conditions.	Adaptable due to probabilistic regularization terms.
Handling Nonlinearities	Highly effective for nonlinear problems, including neural networks.	Effective but may struggle in highly nonlinear spaces.	Addresses nonlinearities through a probabilistic framework.
Sensitivity to Initial Conditions	Less sensitive to initial choices.	Moderately sensitive; influenced by starting point.	Moderately sensitive; choice of priors can impact results.
Computational Efficiency	Deterministic, efficient for small to medium-sized problems.	Deterministic, efficient for many problems, especially with large datasets.	Computationally intensive due to iterative probabilistic updates.
Ease of Use	Requires tuning, yet relatively straightforward to implement.	Fewer hyperparameters, easier to fine-tune.	Requires careful selection of priors and hyperparameters, can be complex.

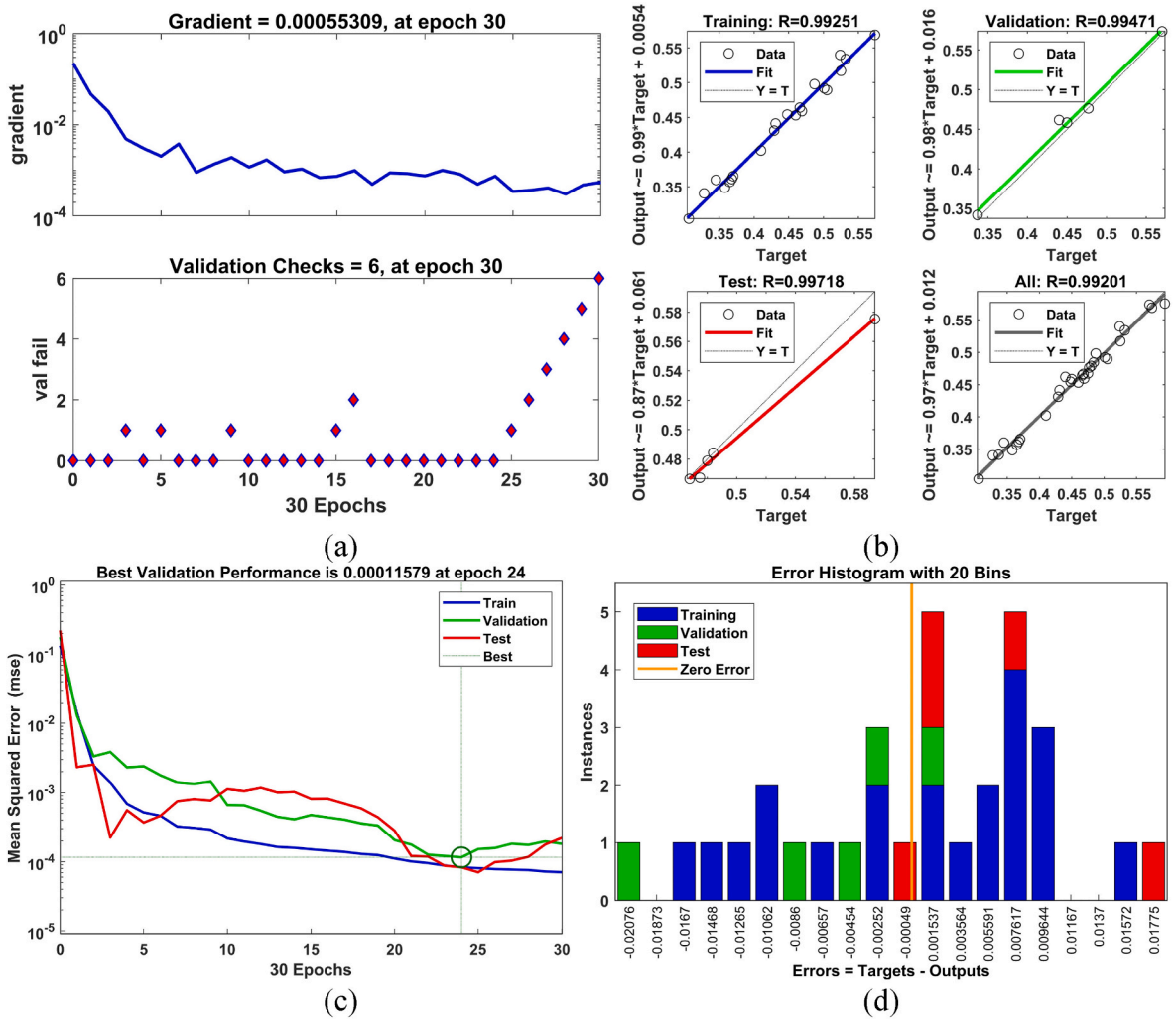

Fig. 5. (a) Training state plot, (b) regression plot, (c) performance plot, (d) error histogram plots obtained by SCG-NN.

0 and advances to Epoch 30, with the objective of attaining the target performance value of 0. Over this period, the performance metric, representing the model's error, decreases significantly from 0.134 to 7.06e-05, indicating substantial improvement. Simultaneously, the gradient, illustrating the steepness of the error surface, diminishes from 0.223 to 0.000553, indicating progressive convergence toward the optimal solution. To ensure consistent performance, six validation checks are conducted throughout the training process. Importantly, the model displays a low mean squared error (MSE) across all datasets, including training (8.3030e-05), validation (1.1579e-04), and test (8.3171e-05), highlighting a robust fit to the data (Table 8). Furthermore, high correlation coefficients (R) are observed, ranging from 0.9925 to 0.9972, indicating a strong and reliable relationship between predicted and actual values across the datasets (Fig. 5).

5. Results and discussion

The KST method's effectiveness was analysed using MATLAB for a 9

Levenberg-Marquardt

```
def train_lmb_ultra_basic(network, data,
target_loss, max_iterations):

  # Initialize weights and biases
  w, b = initialize(network)

  # Hyperparameter
  learning_rate = 0.001
  # Adjust as needed

  for iteration in range(max_iterations):

    # Forward pass (one line)
    output = forward_prop(network, data, w, b)

    # Error calculation (combined)
    error = calculate_error(output, target)

    # Update weights and biases (single step,
simplified)
    w -= learning_rate * error * output
   # Extremely simplified update

  return w, b
```

Bayesian Regularization

```
def train_bayesian_reg_basic(network, data,
epochs, learning_rate, reg_param):

  # Initialize weights and biases
  w, b = initialize(network)

  for epoch in range(epochs):
    for input, target in data:

      # Forward pass (one line)
      output = forward_prop(network, input, w, b)

      # Error calculation (combined)
      error = calculate_error(output, target) +
reg_param * np.sum(w**2)
      # Combine loss and regularization

      # Update weights and biases (simplified)
    w -= learning_rate * update_weights(error, w)
      b -= learning_rate * update_bias(error)

  return w, b
```

Scaled Conjugate Gradient

```
def train_scg_ultra_basic(network, data,
target_loss, max_iterations):

  # Initialize weights and biases
  w, b = initialize(network)

  # Hyperparameter (learning rate)
  learning_rate = 0.001
   # Adjust as needed

  for iteration in range(max_iterations):

    # Forward pass (one line)
    output = forward_prop(network, data, w, b)

    # Error calculation (combined)
    error = calculate_error(output, target)

    # Update weights and biases (single step,
simplified)
    w -= learning_rate * error * output
    # Extremely simplified update

  return w, b
```

Fig. 6. Pseudocode of the proposed LMB, BR, and SCG backpropagation algorithms.

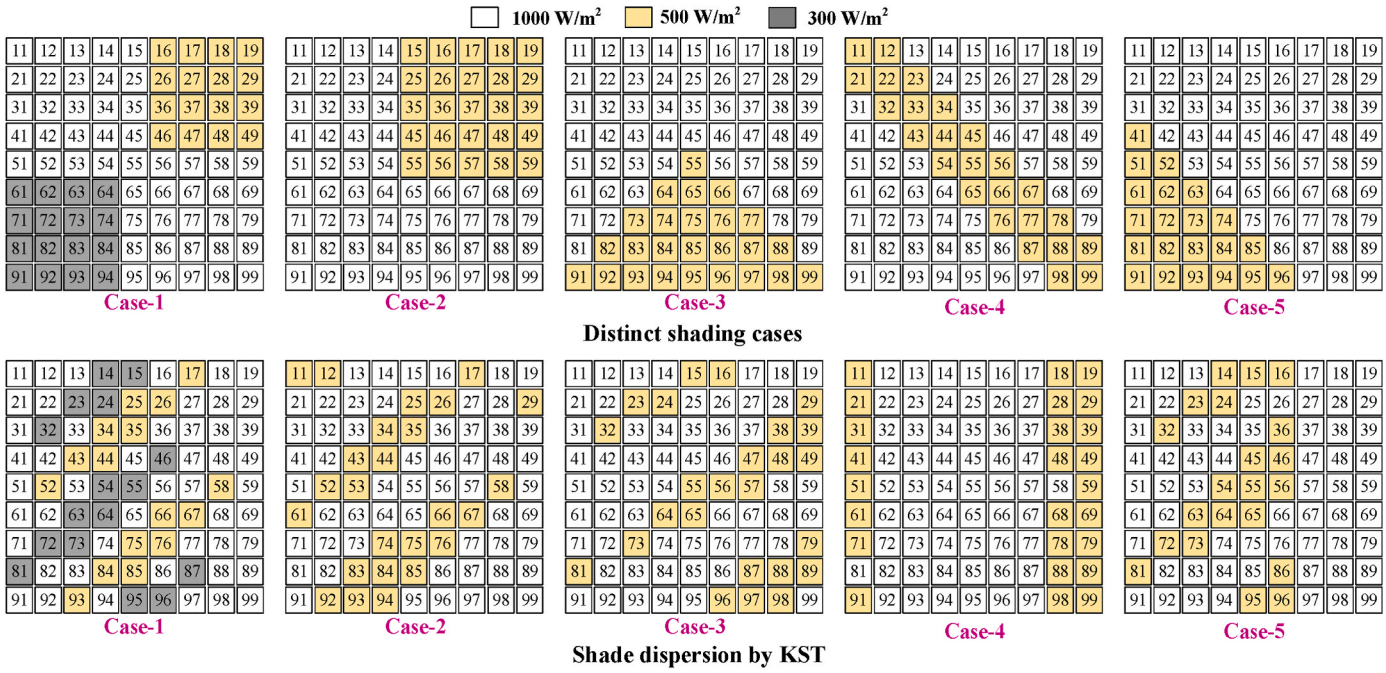

Fig. 7. Different shading cases and their respective distribution of shading effect as obtained by KST.

× 9 PV array. The results were compared with conventional and recently published PV array setups (Velasco-Quesada et al., 2009; Rani et al., 2013; Sahu et al., 2015; Nasiruddin et al., 2019; Reddy and Yammani, 2020; Nihanth et al., 2020; Amar Raj and Anil Naik, 2022) in different shading scenarios. This evaluation utilized a Kyocera Solar KC175GT PV panel exposed to irradiance levels of 1000W/m^2, 500W/m^2, and 300W/m^2, as shown in Fig. 7, for both shaded and unshaded panels. The subsequent sections provide a detailed examination of the proposed configuration, encompassing qualitative and quantitative aspects. Table 10 outlines the Global Maximum Power (GMP) achieved by different layouts of the 9 × 9 array, labelled from Case-1 to Case-5. The power-versus-voltage profiles for these configurations are depicted in Fig. 8. Furthermore, Figs. 9 and 10 illustrate the percentage improvement and the count of peaks observed in the array characteristics for various configurations under these cases, respectively.

5.1. Investigation of shading condition in Case-1

Two sides of the array experience shadow at different degrees of irradiation under Case-1 conditions. By distributing shading evenly among the PV array's rows, the suggested KST approach minimises current variations. The Proposed KST approach achieves the maximum power output of 10696.6 W among various PV array configurations in the Case-1 shading situation (Table 10). The current SDK exhibits variability and inconsistency, performing 6.86% worse than the normal TCT output but failing to consistently surpass TCT in all circumstances. As compared to TCT, the FUP displays a 0.82% reduction, demonstrating uneven performance in terms of yielding noteworthy improvements

Table 10
Obtained GMP (in Kilo Watts) by distinct configurations for a 9x9 array.

Configuration	Case-1	Case-2	Case-3	Case-4	Case-5
TCT (Velasco-Quesada et al., 2009)	1.0271	1.0862	0.8877	1.1963	1.0657
SDK (Rani et al., 2013)	0.9565	1.1792	1.1698	1.1271	1.2172
FUP (Sahu et al., 2015)	1.0186	1.1833	1.1697	1.1619	1.1968
ODE (Nasiruddin et al., 2019)	0.7672	1.1278	1.0597	1.1121	1.1345
OEP (Reddy and Yammani, 2020)	1.0143	1.0615	1.1739	1.1261	1.1379
NAS (Nihanth et al., 2020)	0.8445	1.1257	1.1257	0.9315	1.0657
HMT (Amar Raj and Anil Naik, 2022)	1.0353	1.0863	1.1255	1.1964	1.0699
Proposed KST	**1.0696**	**1.1965**	**1.1789**	**1.1965**	**1.2254**

(Fig. 9). The ODE consistently fails to produce at a level competitive with TCT, falling short of TCT by about 25.30%. The OEP falls short. The OEP is 1.24% behind, which indicates inconsistent delivery of significant improvements over TCT. Furthermore, NAS shows inconsistent results in some circumstances with a 17.77% decrease in GMP when compared to TCT. But in contrast to other methods currently in use, the HMT consistently achieves almost similar performance to TCT, suggesting inconsistently large improvements. In this case, the HMT approach likewise turns out to be ineffective. The proposed KST exhibits consistent performance, outperforming TCT and other existing approaches by a considerable 4.13% when compared to all other existing techniques. In this instance, all currently available methods display several power peaks, usually ranging from 6 to 9 peaks, because of their arbitrary shading dispersion. During GMP tracking, these peaks significantly strain MPPT controllers. By contrast, the suggested KST shows a notable distinction with only three power peak levels. This removes the possibility of becoming stuck in local peaks and lessens the effort on MPPT controllers.

5.2. Investigation of shading condition in Case-2

As seen in Fig. 7, Case 2 subjects one of the corners of the PV array to 500W/m^2 of decreased irradiation. Currently, FUP, SDK, and ODE show gains of 8.93%, 8.56%, and 3.82% above TCT in this situation, indicating performance above the moderate bracket. After these techniques, the NAS approach provides an improvement of 3.63% over the conventional TCT. The HMT method consistently delivers marginal improvements, keeping performance close to par with TCT. However, the OEP performs 2.27% poorer than TCT, demonstrating inconsistent achievement of meaningful improvement. Compared to all other approaches, the suggested KST achieves an impressive 10.15% gain in GMP compared to TCT, exhibiting steady performance with negligible deviations. Owing to suboptimal shade dispersion, existing methods (ODE, OEP, and NAS) produce several peaks and a significant amount of mismatch. On the other hand, as Fig. 8b and 10 show, the suggested KST has better array characteristics with less mismatch.

5.3. Investigation of shading condition in Case-3

In Case 3, we investigate a shading scenario where incident radiation that reaches the lower part of the array is limited by a consistent triangle pattern. The current OEP, SDK and FUP demonstrate a remarkable improvement in Global Maximum Power (GMP) of 32.23%, 31.76% and 31.75% over TCT in this scenario, and their exceptional performance leaves no notable downsides. Furthermore, while there is a slight improvement of 26.80% for the NAS and HMT approaches, their improvement is not as great as it could be for OEP, SDK and FUP. Fig. 9 shows that while ODE has improved over TCT by 19.36%, it is still somewhat limited when compared to other methods. Nonetheless, the suggested KST method surpasses all others, attaining a remarkable 32.79% rise in power production in comparison to TCT, with no notable

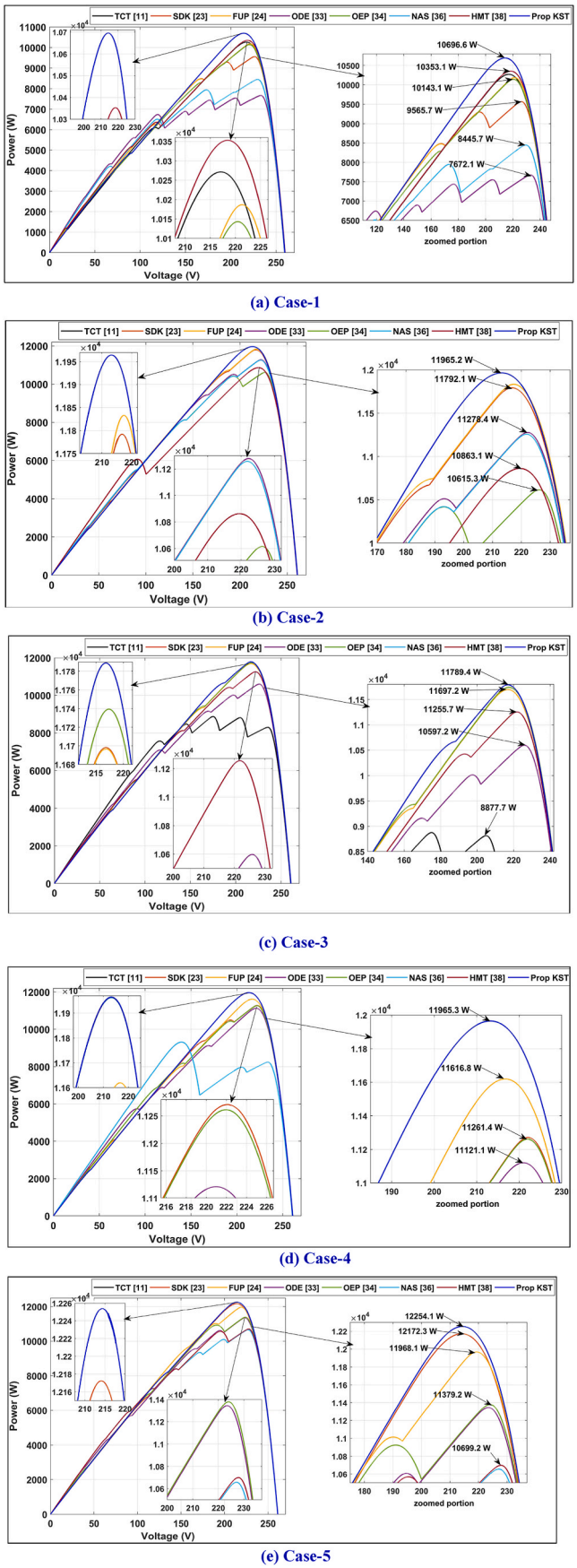

Fig. 8. Power versus voltage characteristics for considered configurations from (a) Case-1 to (e) Case-5.

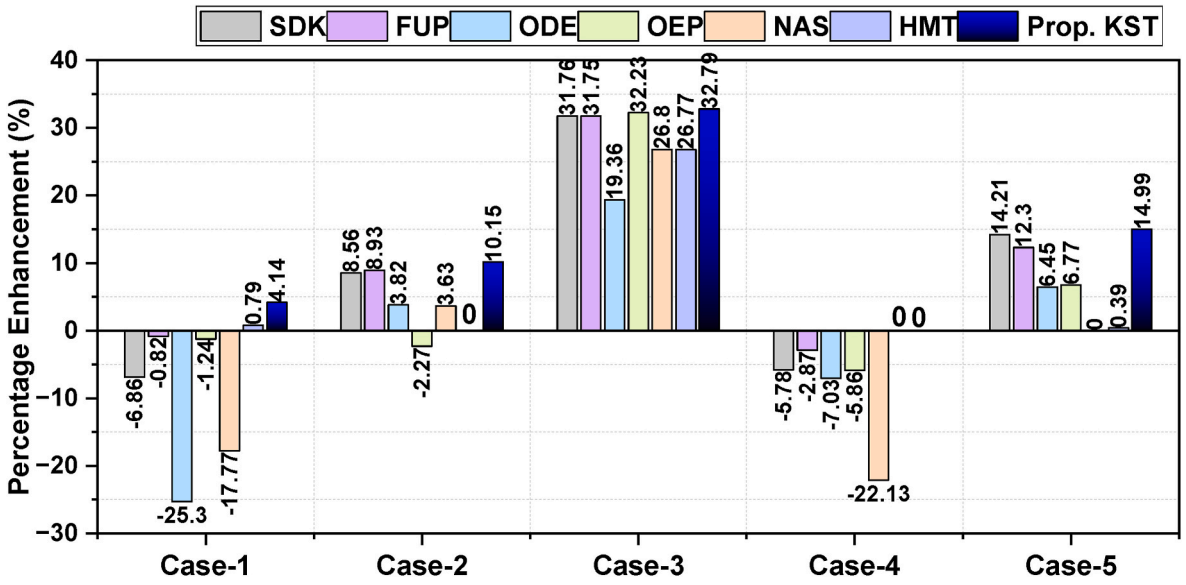

Fig. 9. GMP enhancement of considered configurations during Case-1 to Case-5.

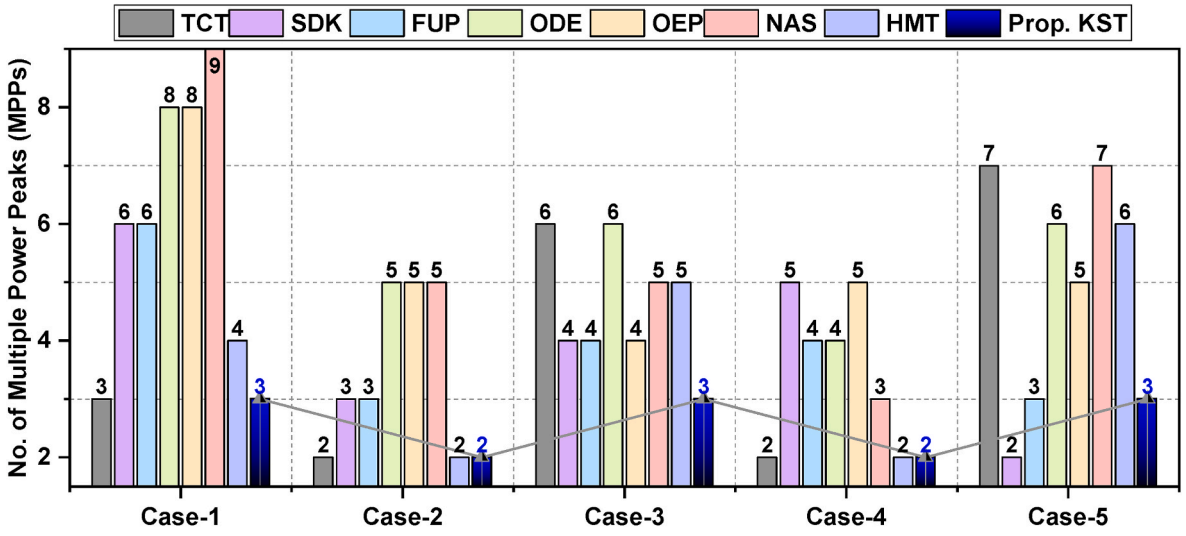

Fig. 10. No. of power peaks exhibited in array characteristics by considered configurations during Case-1-5.

Table 11
Statistical comparison (Wilcoxon Signed-Rank) of each configuration.

Proposed KST vs	R_+	R-	p-value
TCT (Velasco-Quesada et al., 2009)	15	0	0.0431
SDK (Rani et al., 2013)	15	0	0.0431
FUP (Sahu et al., 2015)	15	0	0.0431
ODE (Nasiruddin et al., 2019)	15	0	0.0431
OEP (Reddy and Yammani, 2020)	15	0	0.0431
NAS (Nihanth et al., 2020)	15	0	0.0431
HMT (Amar Raj and Anil Naik, 2022)	10	0	0.0670

disadvantages. Although every current method effectively increases GMP by a significant proportion, power peaks, and mismatch problems are still a problem for them. The array characteristics of all currently used techniques show four to six peaks. However, in comparison to the current ODE and conventional TCT, the suggested technique lowers a number of power peaks by 50%, outperforming other strategies as well.

5.4. Investigation of shading condition in Case-4

As seen in Fig. 7, Case-4 introduces a diagonal shading pattern that affects the array's diagonal part. Although they haven't gotten enough attention in earlier reconfiguration studies, diagonal shading patterns can be found in real-world situations. Only the suggested KST method and the current HMT approaches are able to attain the ideal shade distribution in this scenario. Even when compared to the conventional Total Cross-Tied (TCT) configuration, all other currently used technologies produce noticeably lower Global Maximum Power (GMP), as seen in Fig. 9. More specifically, the GMP decreases in this instance are a result of the current SDK, FUP, ODE, OEP, and NAS approaches showing a significant decline in performance when compared to the traditional TCT configuration, which is 5.78%, 2.87%, 7.03%, 5.86%, and 22.13%, respectively (Fig. 9). This emphasizes that the random reconfiguration process results in large power losses rather than an increase in power production. Because of the mismatch, the indiscriminate shading distribution results in extra losses. The reconfiguration strategy that works best yields consistently better outcomes in a variety of conditions. The suggested KST and HMT approaches, in comparison, exhibit precision

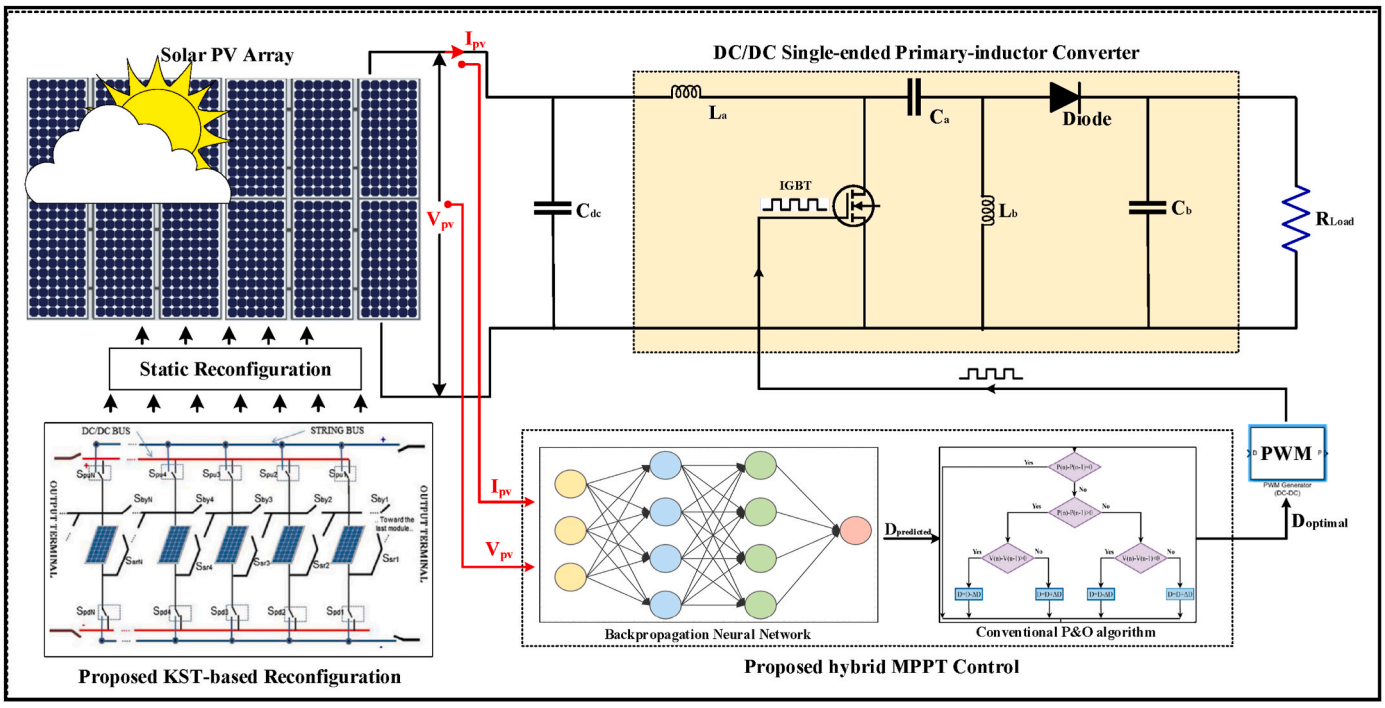

Fig. 11. Description of overall standalone PV system integrated with proposed methodologies.

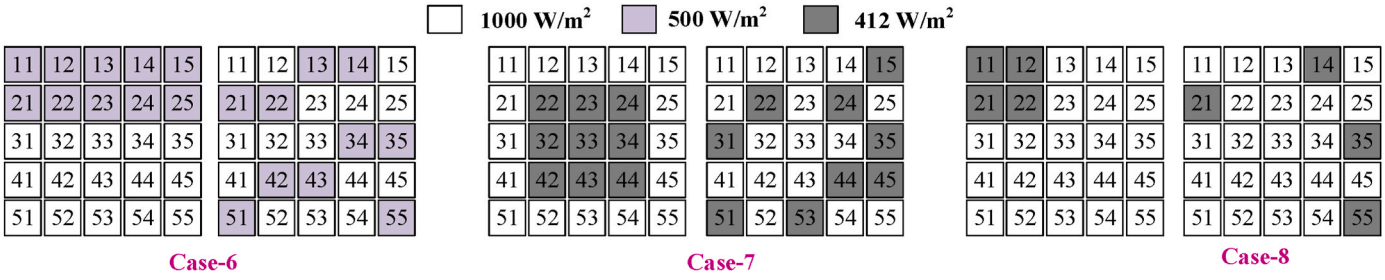

Fig. 12. Shading scenarios examined in the analysis of a 5 × 5 array.

and efficacy consistently without notable irregularities, performing almost as well. Moreover, even in comparison with the benchmark TCT, their performance is significantly worse, mostly because to arbitrary shading dispersion. During GMP tracking, these peaks place a heavy load on MPPT controllers, requiring more sophisticated MPPT trackers. On the other hand, the proposed KST is unique in that it has only two power peaks, which greatly lessens the strain on MPPT controllers and removes the possibility of getting stuck in local peaks. Additionally, it significantly improves the GMP.

5.5. Investigation of shading condition in Case-5

In this case, the corner portion of the array is shaded using a typical triangular shading pattern. In contrast to Cases 1 and 4, the current SDK shows optimal performance with a notable 14.21% improvement over TCT. In contrast to Cases 1 and 4, the FUP approach likewise obtains a significant 12.30% increase over TCT after SDK, showing near-optimal performance. Following the SDK and FUP approaches, improvements of 6.45% and 6.77% are shown for ODE and OEP, respectively. Even though these improvements have some effectiveness, it pales in comparison to SDK and FUP. On the other hand, the current methods for NAS and HMT have a marginal difference of only 0.39%, which indicates inconsistency because they provide performance that is almost equal to one another but not much better. Conversely, the suggested KST exhibits a noteworthy percentage improvement of 14.98% above TCT, indicating steady performance devoid of notable fluctuations. The suggested KST surpasses all other approaches under this shade scenario and achieves the maximum GMP. On the other hand, current methods like ODE, OEP, NAS, and HMT produce less GMP gains and reflect several power peaks, usually in the range of 5–7, which is significantly less than ideal (Fig. 10). Moreover, the current SDK method only improves the GMP by 14.21%, which is equally subpar, even if it produces fewer peaks. The proposed KST in this situation exhibits consistency and efficacy in raising power production and lowering peak occurrences.

To summarise, the KST method outperforms the current approaches (SDK, FUP, ODE, OEP, NAS, HMT) that show variable degrees of performance inconsistency (Fig. 9). These techniques perform well only under a variety of conditions and exhibit very poor performance in other cases. This emphasizes how effective and dependable the KST approach is. Through uniformly distributing concentrated shade impact over the rows, KST ensures regular levels of irradiation and preserves uniformity. Multiple power peaks (MPPs) are less common as a result, and this leads to a less distorted array characteristic. Fig. 8 (a)–(e) and Table 10 vividly demonstrate this result, showing that the KST methodology has fewer MPPs and far smoother characteristics than any other existing methods.

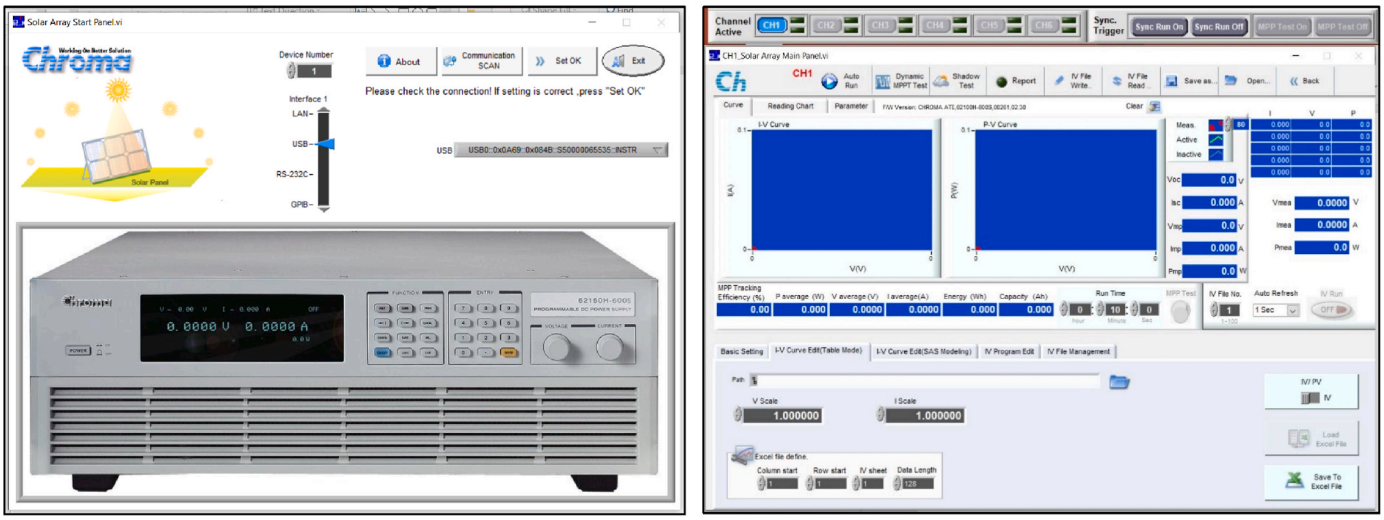

Fig. 13. CHROMA programmable solar PV simulator (left) and its softpanel (right).

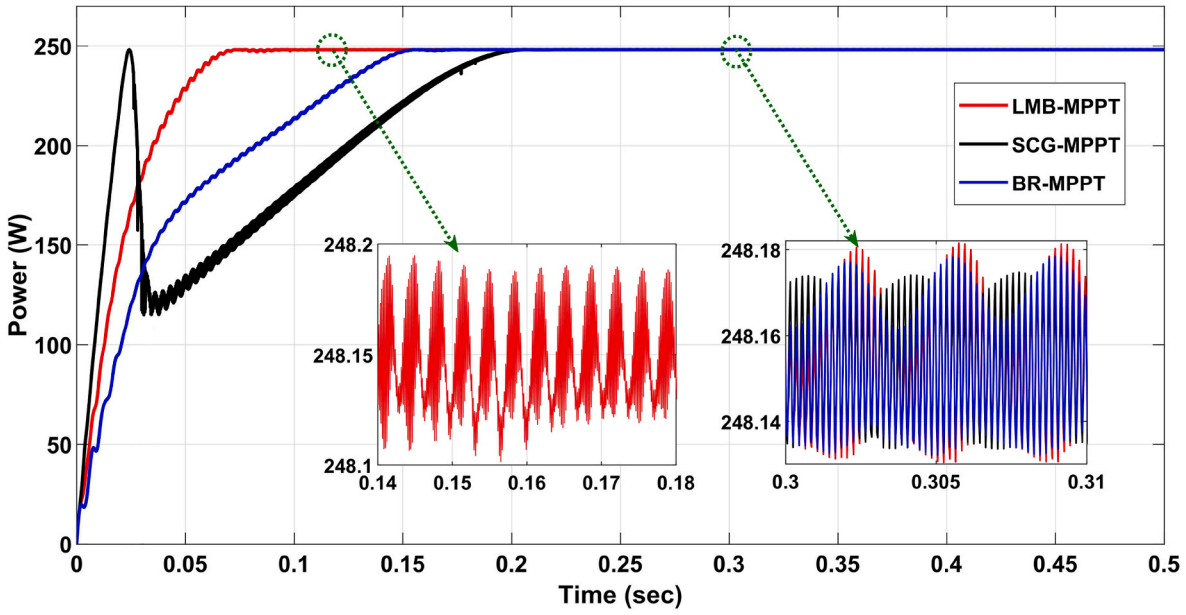

Fig. 14. GMP tracked by LMB, BR, and SCG-MPPT methods under normal (unshaded) conditions.

Table 12
Comparison of the LMB, SCG, BR in terms of Settling time in(sec).

Artificial Neural Network algorithms	Levenberg-Marquardt backpropagation (LMB)	Bayesian Regularization (BR)	Scaled Conjugate Gradient (SCG)
Settling time in (sec)	0.13 s	0.16 s	0.23 s

5.6. Non-parametric performance analysis with wilcoxon test

The Wilcoxon Signed-Rank Test (Bagkavos and Patil, 2021) is a non-parametric method for evaluating performance, especially useful when the data may not follow a normal distribution. It is used to compare whether a new method outperforms an existing one. We employ the non-parametric Wilcoxon Signed-Rank Test ($p < 0.05$) to compare the proposed KST against existing methods (Table 11). This pairwise analysis involves.

Table 13
Obtained GMP by Chroma simulator and simulation studies for a 5x5 array.

Case	GMP (W) Before Reconfiguration		GMP (W) After Reconfiguration		% Enhancement
	Simulation	Chroma data	Simulation	Chroma data	
Case-6	143.9	146.5	197.3	199.0	~37.10
Case-7	167.1	168.5	191.1	192.7	~14.36
Case-8	201.3	203.1	221.2	223.0	~9.88

- Obtain the GMP values for all configurations across shading conditions.
- Calculating positive ranks ($R+$) where KST achieves higher GMP.
- Calculating negative ranks ($R-$) where existing methods outperform KST.

Table 14
Evaluation of lmb-MPPT performance against established MPPT algorithms.

Parameter	ACO-NPU (Deboucha et al., 2021)	ACO-NPU PSO (Deboucha et al., 2021)	JAYA (Deboucha et al., 2020)	GWO (Houssein et al., 2021)	LPSO (Makhloufi and Mekhilef, 2021)	Proposed LMB
Tracking time (sec)	2.15	1.3	2.85	1.3	20	**0.13**
Tracking efficiency in %	98.6	99.67	99.21	98.90	97.01	**99.48**
Execution complexities	Complex	Complex	Medium	Complex	Complex	**Relatively Simple**
Complexity	Very High	Very High	High	High	High	**Very Low**
Tracking oscillations	Medium	Low	Low	Medium	Medium	**Low**
Susceptibility to local minima/maxima	Medium	Medium	Medium	Medium	Medium	**Low**

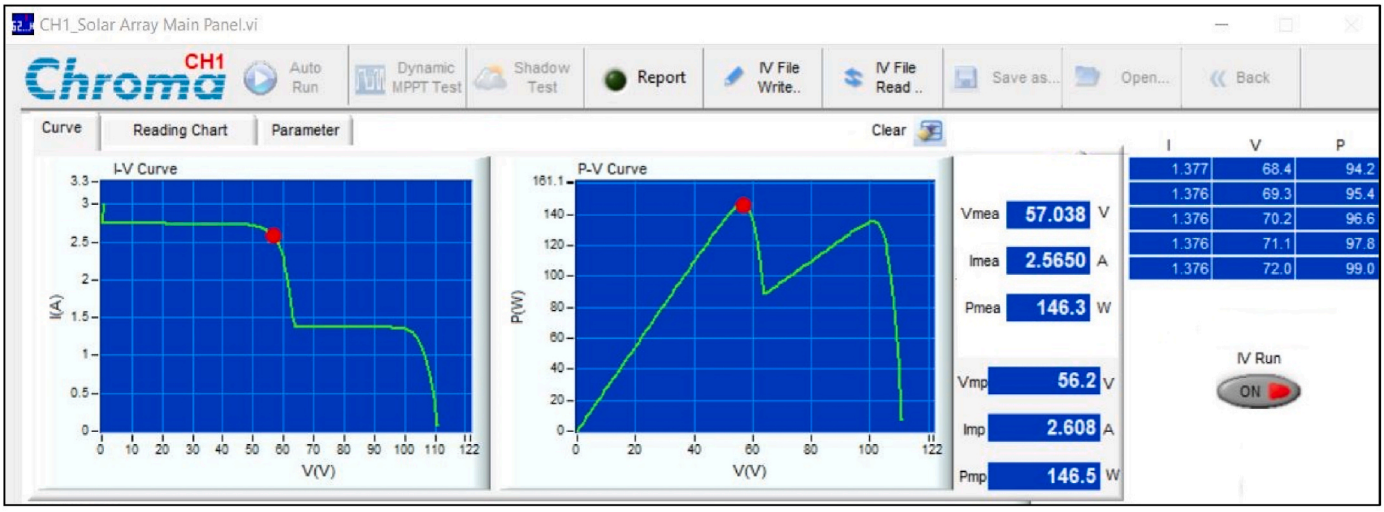

(a) Before reconfiguration

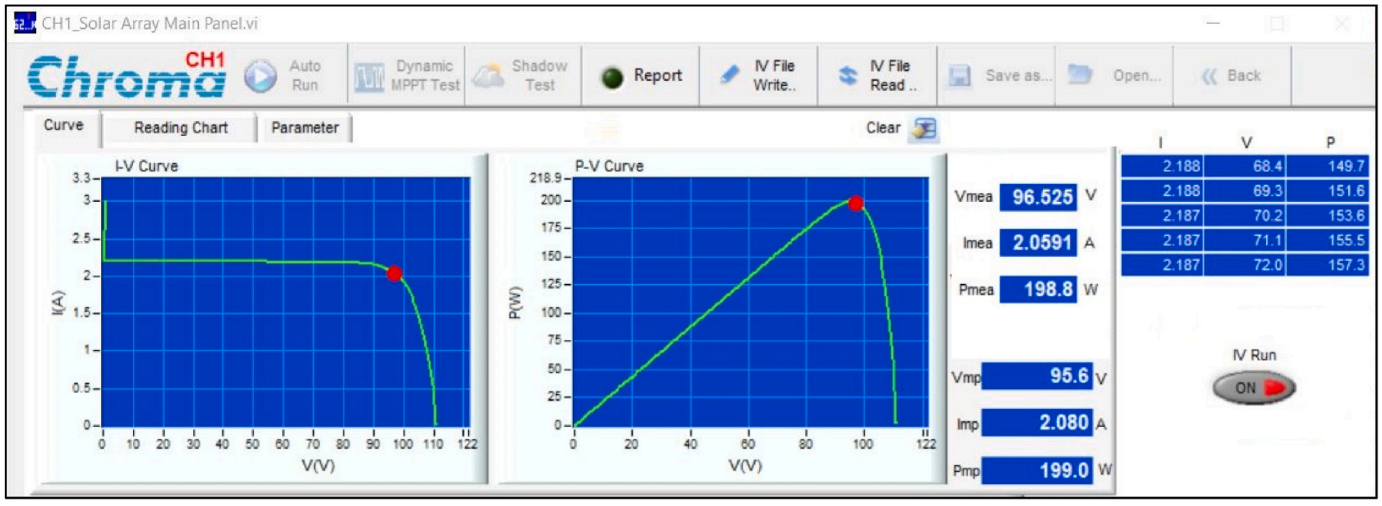

(b) After reconfiguration

Fig. 15. IV and PV curves obtained by CHROMA 62100H–600S under Case-6.

- Determining the p-value to assess the statistical significance of the results. A lower p-value ($p < 0.05$) indicates a statistically significant difference between KST and existing methods, supporting its effectiveness.

Table 11 results confirm KST's superiority over existing methods, as evidenced by p-values strictly less than 0.05. TCT (Velasco-Quesada et al., 2009), SDK (Rani et al., 2013), FUP (Sahu et al., 2015), ODE (Nasiruddin et al., 2019), OEP (Reddy and Yammani, 2020), NAS (Nihanth et al., 2020): The p-value for these configurations is 0.0431, which is statistically significant at a 5% level. This suggests that KST performs statistically better than these configurations. Consistently high positive ranks (R+) for KST indicate it achieves the highest GMP across all array sizes. While HMT (Amar Raj and Anil Naik, 2022) exhibits a better p-value of 0.0670 compared to the existing ones, its performance fails to be efficient under column shading conditions. Further, in all the four test cases, HMT yields significantly lower GMP compared to proposed KST. In contrast, KST maintains consistently high performance

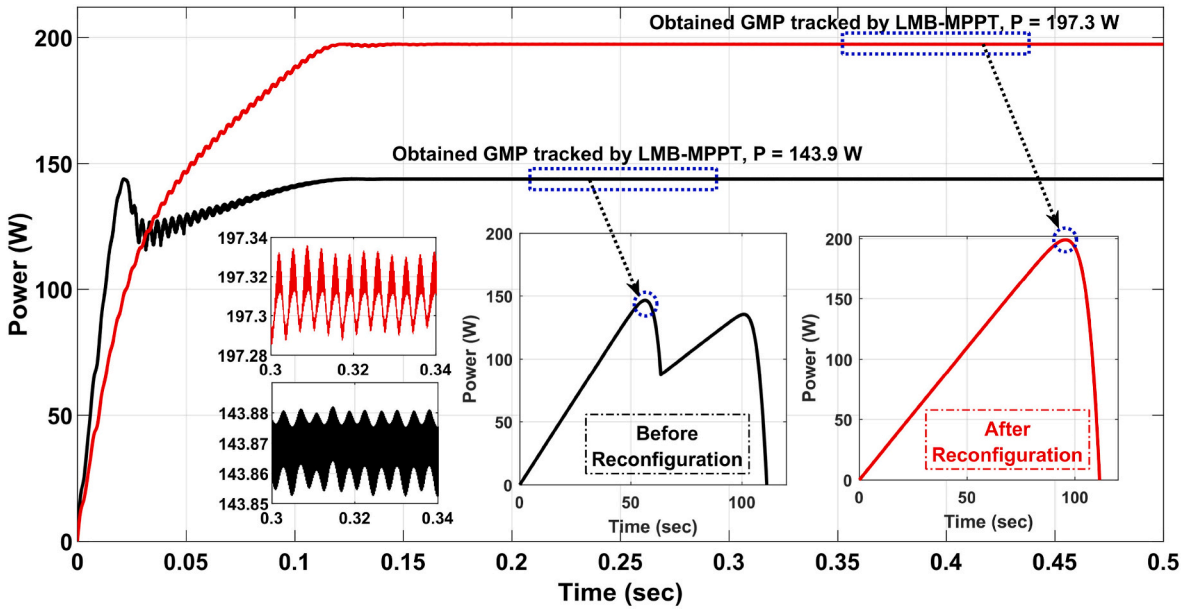

Fig. 16. GMP tracked by proposed hybrid LMB- MPPT under Case-6.

across all array sizes and shading scenarios. This confirms KST's superiority as the most effective method.

6. Assessment using a hybrid MPPT controller based on LMB-PO algorithm

During any shading condition or low irradiance, mismatch losses increase and the array exhibits multiple peaks. The electrical circuitry of the panels is configured according to the encrypted matrix obtained by the KST strategy, as shown in Fig. 11. After this one-time static/fixed reconfiguration process, if the array experiences any shading, the concentrated shade is dispersed, enhancing the GMP, reducing mismatch, and eliminating the multiple peaks. The proposed LMB-based MPPT controller, integrated into the system, tracks the enhanced GMP easily due to the elimination of multiple peaks, with lower steady-state oscillations and higher accuracy. In this way, the employment and integration of both the proposed KST reconfiguration strategy and the LMB-based MPPT controller in the overall system enhances the GMP and tracking accuracy. The hybrid LMB-P&O MPPT approach is applied on a reconfigured array in this validation operation. The configuration combines a dc-dc SEPIC converter and a resistive load with a resistance of 159.2Ω, as shown in F ig. 23 The 64-bit version of the R2022b-MATLAB environment was used for testing and numerical analysis. The ode23tb stiff/TR-BDF2 variable-step type solver was used, and the tolerance level was set to 1e-05. The specifications of the converter were considered, which included a switching frequency defined at 5000 Hz and a DC link capacitance of 50 μF. Moreover, the capacitance of the SEPIC converter (C_a and C_b) was determined to be 178 μF and 89 μF, respectively, and its inductance (L_a and L_b) was calculated as 1.95 mH (refer to Table 1). The effectiveness of the proposed KST reconfiguration algorithm, when combined with the LMB-based MPPT approach, was evaluated across various shading scenarios. The MATLAB Simulink model of the overall system is Fig. 23 of Appendix.

Three shading scenarios are considered in order to assess and show how well the reconfiguration algorithm integrated with the LMB-MPPT controller works (see Fig. 11). Both shaded and unshaded panels were subjected to irradiance intensities of 1000W/m^2, 500W/m^2, and 412W/m^2 (Fig. 12). The GMP obtained was simulated using the proposed KST method. The simulation results were then contrasted with the array's Current-Voltage (IV) and Power-Voltage (PV) characteristics generated by Chroma solar array simulator (Fig. 13). A thorough examination of the system's operation in the following sections for various shading scenarios.

The optimized duty cycle for GMP tracking has been determined using three distinct Backpropagation algorithms: LMB, SCG, and BR. Information from Table 13 and the analysis in Fig. 14 reveals that the LMB method, utilized for MPPT, efficiently tracks GMP within a short period when compared to the SCG and BR algorithms (shown in Table .12). Additionally, all three methods maintain GMP with minimal oscillations, ranging from 248.13W to 248.18W, an insignificantly small range. Despite the effective GMP tracking with lower oscillations, both SCG and BR methods require a relatively longer duration for the tracking process. Consequently, in this study, we have chosen to employ the LMB method for GMP tracking in the reconfigured PV array.

From Case 6 to Case 8, the array encounters shading conditions, typically characterized by distinct square and rectangular shading patterns illustrated in Fig. 12. In this scenario, the irradiance levels for unshaded and shaded panels are 1000W/m^2, 500W/m^2, and 412W/m^2. This variation in irradiance levels among PV array rows leads to the presence of numerous local maximum power points (LMPP) in the characteristics. However, by employing the proposed KST procedure for reconfiguration, this LMPP issue is effectively resolved, resulting in just a single power peak (as shown in Fig. 15, Fig. 17 and Fig. 19). As evidenced in Figs. 16, 18 and 20, this simplifies the tracking of the Global Maximum Power (GMP) and significantly reduces tracking oscillations. The reconfigured array displays significantly smoother characteristics thanks to the implementation of an intelligent shadow dispersion technique. This enhancement enables the array to effectively track GMP values of 197.3W, 191.1W, and 221.1W in shading Cases 6 through 8, respectively. When we compare GMP tracking after reconfiguration in each of these scenarios to the array's performance before reconfiguration, we observe improvements of 37.10%, 14.36%, and 9.88%, respectively. Fig. 14 through 20 illustrate that the PV characteristics obtained through simulation and the Chroma software closely align, affirming the feasibility and practicality of the proposed KST.

- ACO-NPU (Deboucha et al., 2021) is effective for optimization problems, but new pheromone update rules can cause drawbacks like premature convergence, increased tuning complexity, potential instability, and unpredictable behaviour. Balancing exploration and exploitation is also challenging, which can hinder the overall performance.

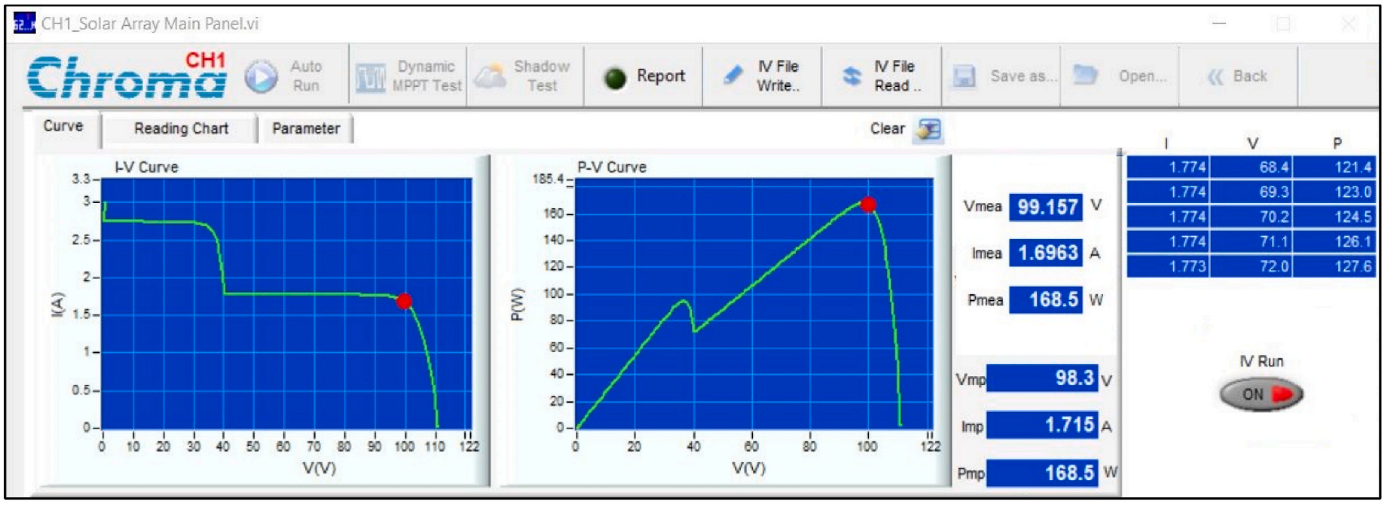

(a) Before reconfiguration

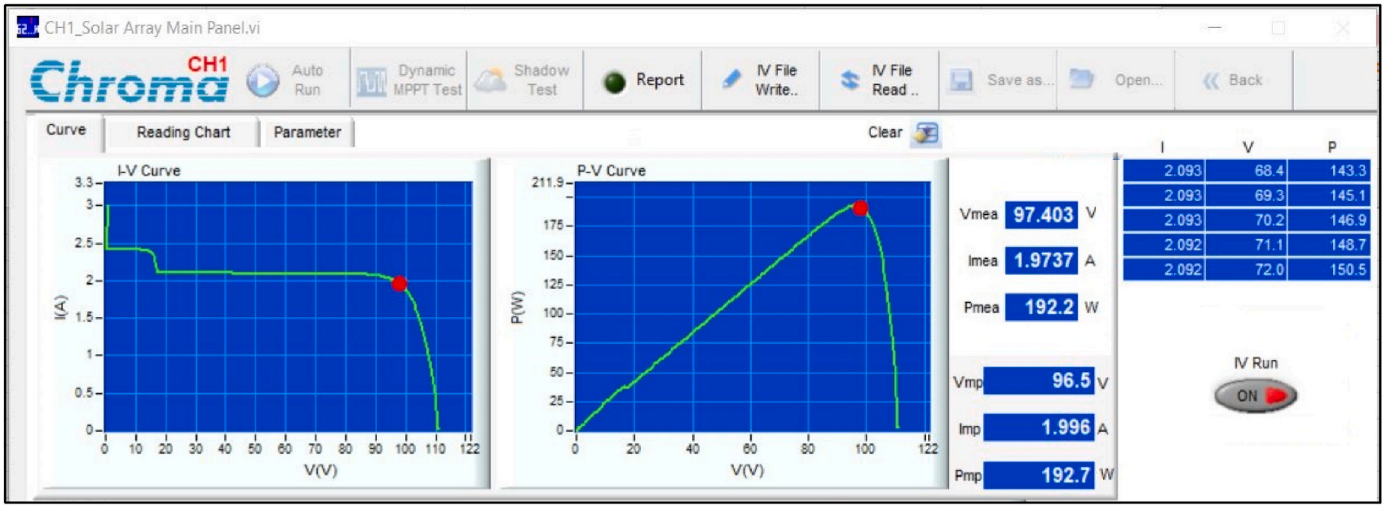

(b) After reconfiguration

Fig. 17. IV and PV curves obtained by CHROMA 62100H–600S under Case-7.

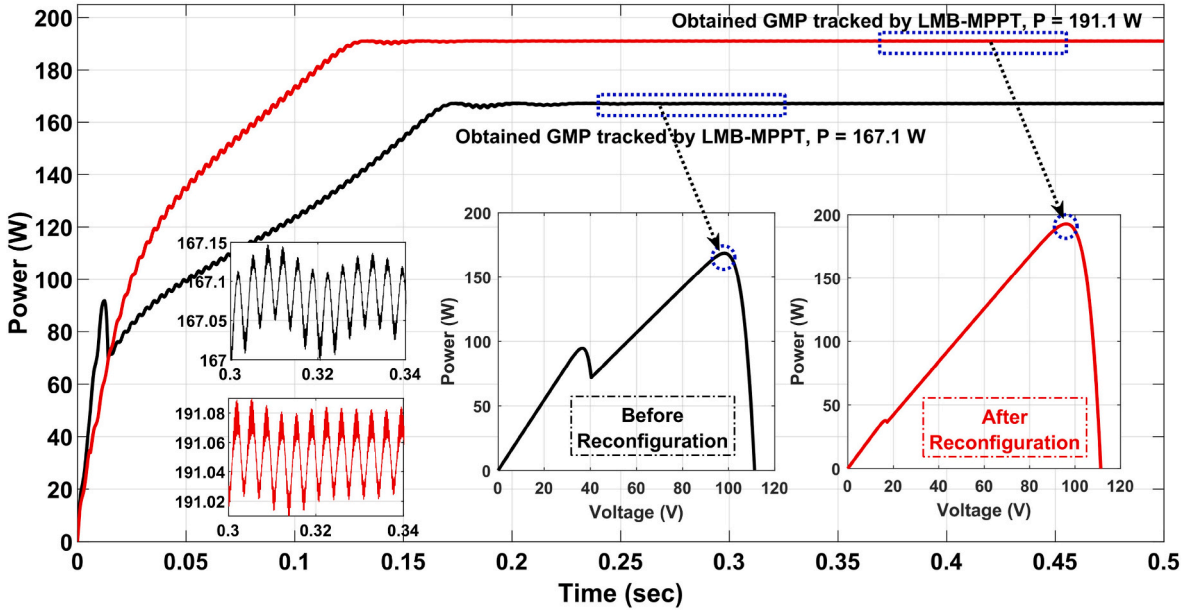

Fig. 18. GMP tracked by proposed hybrid LMB-MPPT under Case-7.

- The ACO-NPU-PSO introduced in (Deboucha et al., 2021) obtained by combining search strategies in ACO and PSO presents challenges. The conflicting update mechanisms require careful design to avoid confusing the agents. Tuning the control parameters of both algorithms can be complex and time-consuming. It is also manifested in the GMP tracking time as shown in Table .14. The tracking time obtained by the proposed neural network-based LMB controller is around 0.13sec which is significantly less compared to the existing ACO-NPU and ACO-NPU PSO which is around 2.15sec and 1.3sec respectively. Additionally, a larger population of agents may be needed, increasing computational costs. There is also a risk of information overload from combining pheromone trails and particle positions, which can hinder the agents' decision-making process.
- The JAYA-based MPPT controller (Deboucha et al., 2020), while simple, suffers from slow convergence in complex problems, limited exploration potentially missing better solutions, and sensitivity to the initial population. The obtained tracking time by JAYA algorithm is 2.85sec which is also comparatively more. Its theoretical foundation is less developed, and limited parameter tuning hinders fine-tuning for specific problems.
- The GWO-based MPPT (Houssein et al., 2021) may exhibit slow convergence, vulnerability to local optima, and could potentially benefit from a more diverse initial population. Additionally, the limited options for parameter tuning could restrict its ability to finely adjust to specific problem requirements.
- The Logarithmic Particle Swarm Optimization (LPSO) shares PSO's slow convergence in complex problems despite its logarithmic inertia weight (Makhloufi and Mekhilef, 2021). LPSO takes around 10sec which is too long to track the GMP (Table .14). It can prematurely converge to local optima and requires careful parameter tuning. Balancing exploration and exploitation with the logarithmic inertia weight remains a challenge, influenced by specific problem characteristics.

Many existing partial shading studies (e.g. (Subha and Himavathi, 2018; Aldair et al., 2018; Chen and Wang, 2019),) rely on neural networks trained with sensor data. Typically, these networks use irradiation and temperature as inputs (Fig. 21). However, most simulations (e.g. (Subha and Himavathi, 2018; Aldair et al., 2018; Chen and Wang, 2019),) employ simplified PV array models in MATLAB that assume uniform irradiation and temperature across all modules. This approach (e.g., 5 parallel strings, 3 series modules) is unrealistic as it doesn't capture the variations in real-world shading scenarios (Fig. 22). In reality, modules experience different irradiation levels, especially under partial shading. To accurately analyze real-time partial shading, a more detailed model with series and parallel connections is necessary (Fig. 22). Existing studies on MPPT controllers using neural networks often rely on a single PV array block in simulation, requiring only irradiation and temperature sensors (limited practicality). However, for real-world analysis with multiple panels, each would need individual irradiation and temperature sensors, leading to a significant increase with array size (e.g., 25 sensors for a 5×5 array. In contrast, our controller in proposed strategy (Fig. 22) leverages the array's total voltage and current for training, requiring only two sensors regardless of array size. This significantly reduces sensor requirements compared to existing methods, whose needs grow exponentially with larger arrays.

7. Conclusions

This study introduces an innovative reconfiguration approach inspired by the Kolakoski Sequence Transform (KST) and leverages image encryption techniques to optimize shading loss reduction. The proposed KST strategy effectively addresses the shortcomings of existing methods and has been rigorously validated across 9×9 and 5×5 photovoltaic arrays subjected to 8 shading scenarios. Comparative assessments against seven established configurations demonstrate that the KST configuration outperforms them, resulting in enhancements of 37.10%, 32.79%, 14.98%, 14.36% and 10.15% in the GMP for various shading conditions. The distinctive aspect of the KST technique is its capability to evenly distribute shading, resulting in reduced correlations between adjacent shaded panels within an array and minimizing current discrepancies between rows. This unique characteristic contributes to achieving the highest GMP and enhancing array performance, consequently reducing the demand on MPPT controllers. The algorithm's

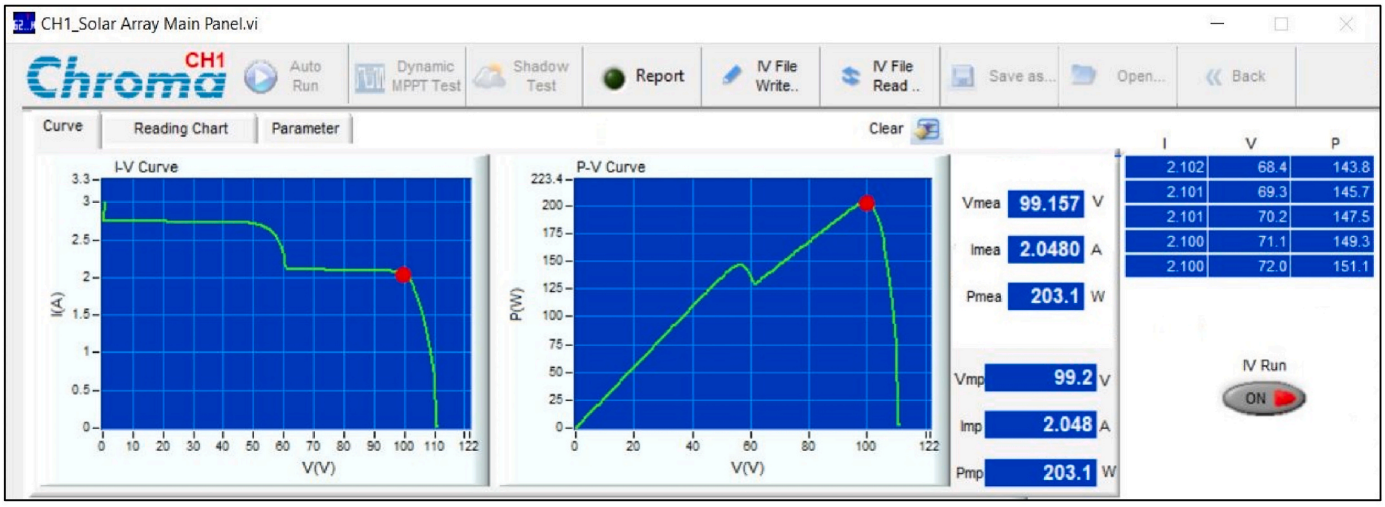

(a) Before reconfiguration

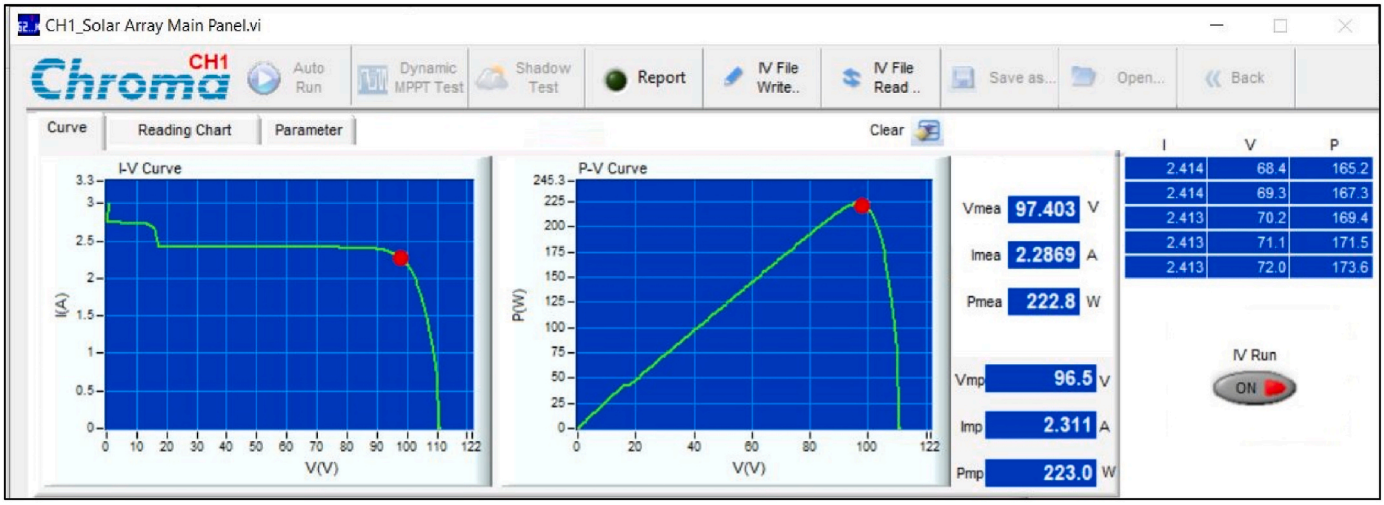

(b) After reconfiguration

Fig. 19. IV and PV curves obtained by CHROMA 62100H–600S under Case-8.

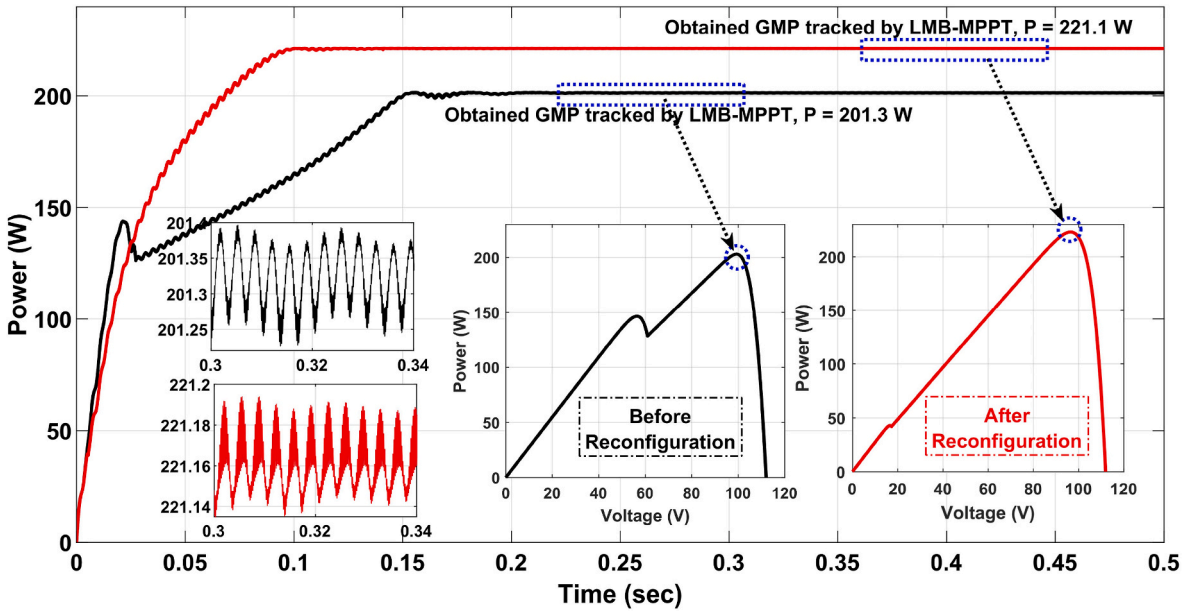

Fig. 20. GMP tracked by proposed hybrid LMB-MPPT under Case-8.

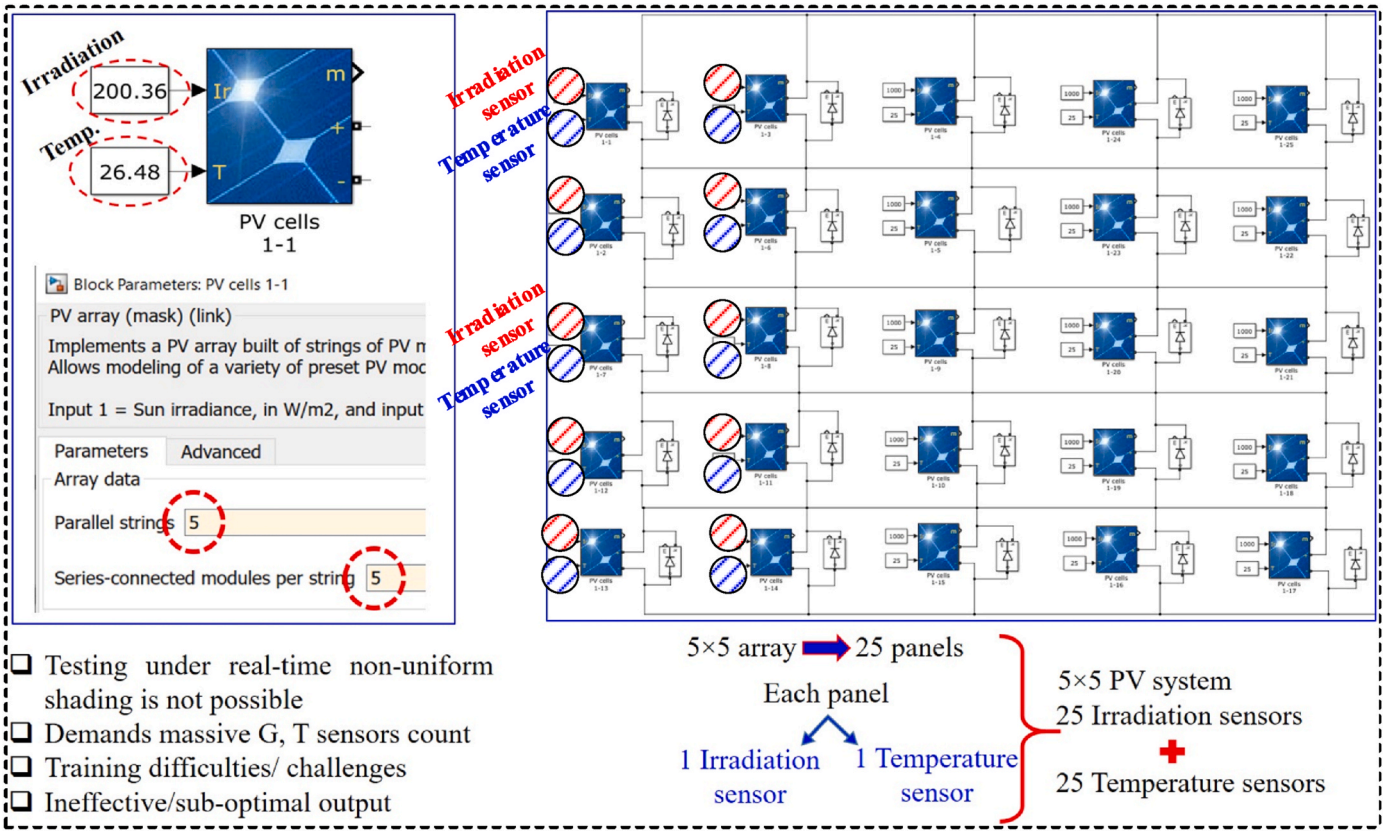

Fig. 21. Requirement of numerous sensors necessitated for GMP tracking by existing methods (Subha and Himavathi, 2018; Aldair et al., 2018; Chen and Wang, 2019).

integration with an LMB-based MPPT controller for a 250Wp standalone PV system exposed to various shading circumstances serves as additional evidence of its efficacy. Increased GMP, smoother array performance, and consistently low mismatch highlight the suggested approach's dependability and effectiveness in compared to alternative approaches. Furthermore, three different artificial neural network methods have been studied in detail for MPPT, The Levenberg-Marquardt, Scaled Conjugate Gradient, and Bayesian Regularization algorithms. The suggested combined reconfiguration-MPPT technique has the best likelihood of successfully eliminating shading effects, according to a detailed quantitative and qualitative investigation.

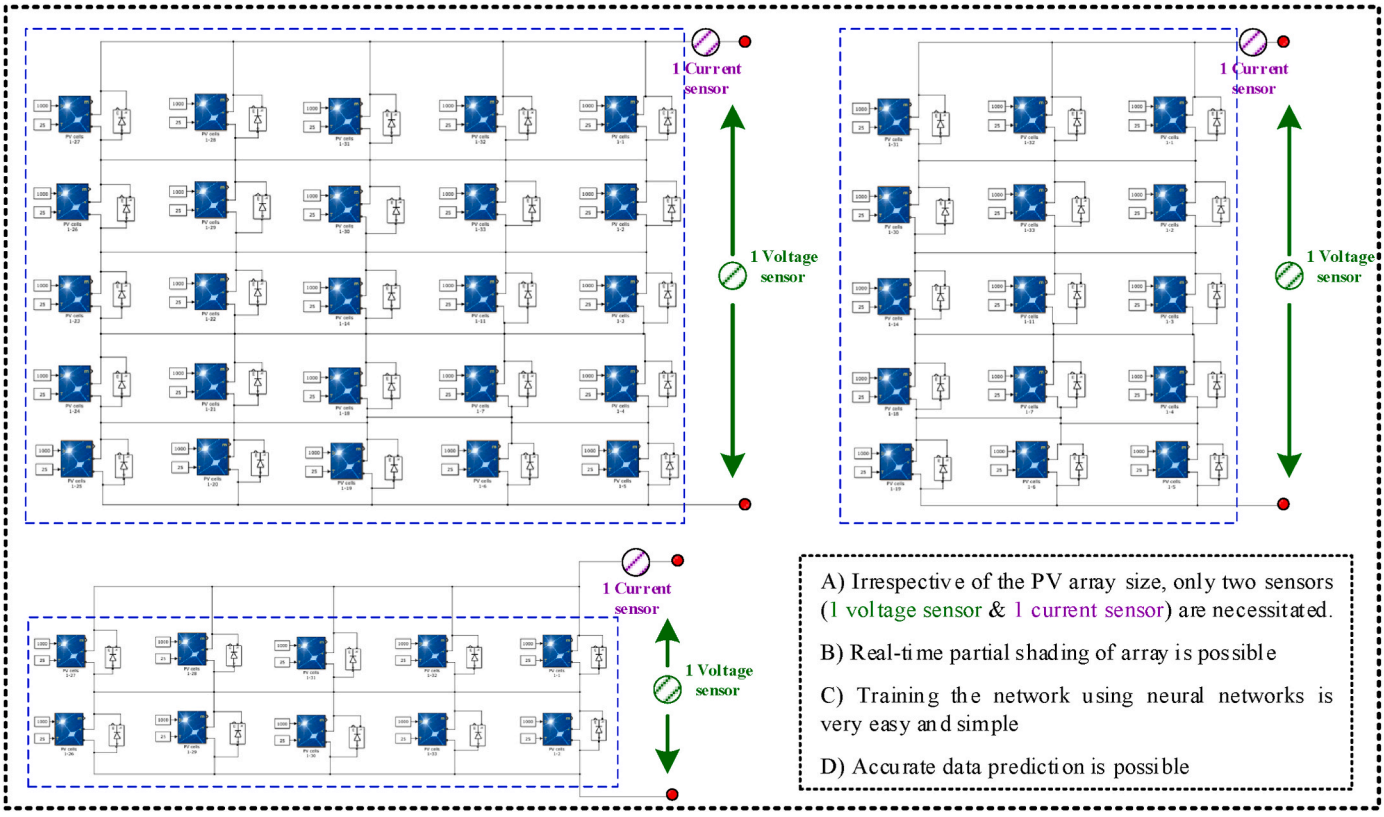

Fig. 22. Proposed methodology requiring only two sensors irrespective of array size.

Statement on potential conflicts of interest

The authors have declared that they have no competing interests to disclose.

CRediT authorship contribution statement

Madavena Kumaraswamy: Writing – review & editing, Writing – original draft, Validation, Software, Methodology, Investigation, Conceptualization. **Kanasottu Anil Naik:** Writing – review & editing, Supervision, Software, Resources.

Declaration of competing interest

The authors declare that they have no known competing financial interests or personal relationships that could have appeared to influence the work reported in this paper.

Data availability

Data sharing is not applicable to this article as there were no new data generated or analyzed in the course of this study.

Appendix

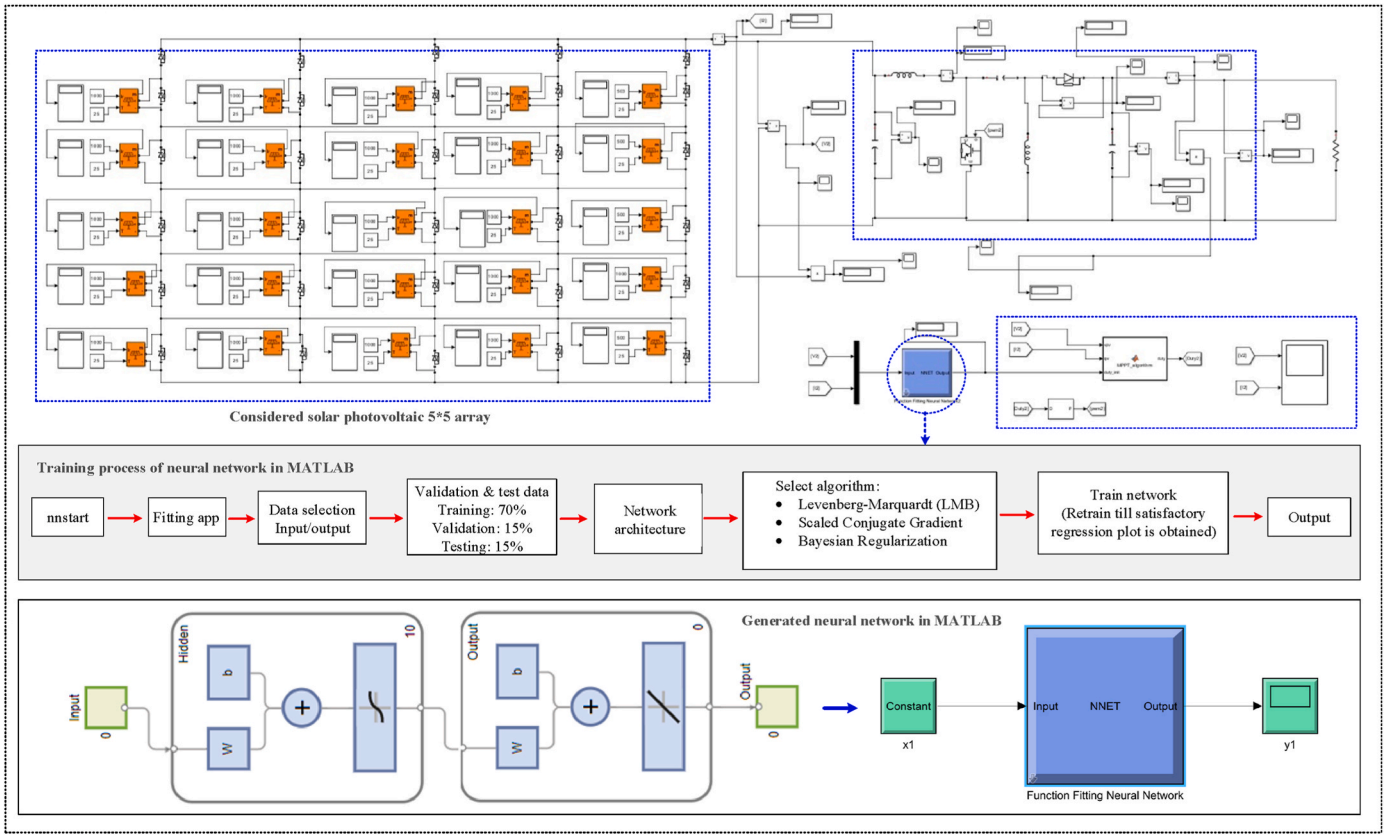

Fig. 23. MATLAB Simulink model of the overall system.

References

Ahmed, Fathy, Rezk, Hegazy, Yousri, Dalia, 2020. A robust global MPPT to mitigate partial shading of triple-junction solar cell-based system using manta ray foraging optimization algorithm. Sol. Energy 207, 305–316. https://doi.org/10.1016/j.solener.2020.06.108. ISSN 0038-092X.

Ahmed, S., Mekhilef, S., Mubin, M., Tey, K.S., Kermadi, M., 2023. An adaptive perturb and observe algorithm with enhanced skipping feature for fast global maximum power point tracking under partial shading conditions. IEEE Trans. Power Electron. 38 (9), 11601–11613. https://doi.org/10.1109/TPEL.2023.3285243.

Aldair, A.A., Obed, A.A., Halihal, A.F., 2018. Design and implementation of ANFIS-reference model controller based MPPT using FPGA for photovoltaic system. Renew. Sustain. Energy Rev. 82, 2202–2217.

Aljafari, B., Satpathy, P.R., Thanikanti, S.B., Haes Alhelou, H., 2023. A zero switch and sensorless reconfiguration approach for sustainable operation of roof-top photovoltaic system during partial shading. IET Renew. Power Gener. 17 (6), 1385–1412.

Alshareef, M.J., 2022. An effective falcon optimization algorithm based MPPT under partial shaded photovoltaic systems. IEEE Access 10, 131345–131360. https://doi.org/10.1109/ACCESS.2022.3226654.

Amar Raj, R.D., Anil Naik, K., 2022. A generalized henon map-based solar PV array reconfiguration technique for power augmentation and mismatch mitigation. IETE J. Res. 1–19.

Amar Raj, R.D., Naik, K.A., 2022. A novel solar photovoltaic array reconfiguration technique using two-dimensional generalized Arnold's cat map. J. Sol. Energy Eng. 144 (6), 061001.

Amar Raj, R.D., Naik, K.A., 2023. Solar array optimization using cryptographic fibonacci transformation for global power enhancement and ease of MPPT controllers. Energy Technol. 11 (9), 2300380 https://doi.org/10.1002/ente.202300380.

Anjum, S., Mukherjee, V., Mehta, G., 2021. Advanced SuDoKu-based reconfiguration strategies for maximum power extraction from partially shaded solar photovoltaic array. J. Sol. Energy Eng. 143 (6), 061003.

Anjum, S., Mukherjee, V., Mehta, G., 2022. Hyper SuDoKu-based solar photovoltaic array reconfiguration for maximum power enhancement under partial shading conditions. J. Energy Resour. Technol. 144 (3), 031302.

Bagkavos, Dimitrios, Patil, Prakash N., 2021. Improving the Wilcoxon signed rank test by a kernel smooth probability integral transformation. Stat. Probab. Lett. 171, 109026 https://doi.org/10.1016/j.spl.2020.109026. ISSN 0167-7152.

Bouselham, L., Rabhi, A., Hajji, B., Mellit, A., 2021. Photovoltaic array reconfiguration method based on fuzzy logic and recursive least squares: an experimental validation. Energy 232, 121107.

Chandrasekharan, Sowthily, Subramaniam, Senthilkumar, Veerakgoundar, Veeramani, 2023. Honey badger optimization algorithm based maximum power point tracking for solar photovoltaic systems. Elec. Power Syst. Res. 221, 109393 https://doi.org/10.1016/j.epsr.2023.109393. ISSN 0378-7796.

Chen, L., Wang, X., 2019. Enhanced MPPT method based on ANN-assisted sequential Monte–Carlo and quickest change detection. IET Smart Grid 2 (4), 635–644.

de Jesús Rubio, J., 2020. Stability analysis of the modified Levenberg–Marquardt algorithm for the artificial neural network training. IEEE Transact. Neural Networks Learn. Syst. 32 (8), 3510–3524.

Deboucha, H., Mekhilef, S., Belaid, S., Guichi, A., 2020. Modified deterministic Jaya (DM-Jaya)-based MPPT algorithm under partially shaded conditions for PV system. IET Power Electron. 13 (19), 4625–4632.

Deboucha, H., Shams, I., Belaid, S.L., Mekhilef, S., 2021. A fast GMPPT scheme based on collaborative swarm algorithm for partially shaded photovoltaic system. IEEE Journal of Emerging and Selected Topics in Power Electronics 9 (5), 5571–5580.

Ding, M., Li, H., Zhao, L., Yang, D., 2023. A high-performance isolated bridgeless resonant SEPIC PFC converter at medium line frequencies. IEEE Trans. Power Electron. 38 (8), 10040–10051. https://doi.org/10.1109/TPEL.2023.3279610.

Guo, Z., Yang, B., Chen, Y., Li, Z., Li, Q., Deng, J., Guo, C., Zhang, X., Tang, B., Zhu, M., Qu, S., 2023. Modular thermoelectric generation arrays reconfiguration under heterogeneous temperature distribution via improved cooperation search algorithm: modelling, design and HIL validation. Appl. Therm. Eng. 219, 119323.

Houssein, E.H., Mahdy, M.A., Fathy, A., Rezk, H., 2021. A modified Marine Predator Algorithm based on opposition based learning for tracking the global MPP of shaded PV system. Expert Syst. Appl. 183, 115253.

Ibrahim, S.A., Nasr, A., Enany, M.A., 2021. Maximum power point tracking using ANFIS for a reconfigurable PV-based battery charger under non-uniform operating conditions. IEEE Access 9, 114457–114467.

Khadse, C.B., Chaudhari, M.A., Borghate, V.B., 2016. Electromagnetic compatibility estimator using scaled conjugate gradient backpropagation based artificial neural network. IEEE Trans. Ind. Inf. 13 (3), 1036–1045.

Krishna, G.S., Moger, T., 2019a. Improved SuDoKu reconfiguration technique for total-cross-tied PV array to enhance maximum power under partial shading conditions. Renew. Sustain. Energy Rev. 109, 333–348.

Krishna, S.G., Moger, T., 2019b. Optimal SuDoKu reconfiguration technique for total-cross-tied PV array to increase power output under non-uniform irradiance. IEEE Trans. Energy Convers. 34 (4), 1973–1984.

Makhloufi, S., Mekhilef, S., 2021. Logarithmic PSO-based global/local maximum power point tracker for partially shaded photovoltaic systems. IEEE Journal of Emerging and Selected Topics in Power Electronics 10 (1), 375–386.

Mansoor, Majad, Feroz Mirza, Adeel, Ling, Qiang, Yaqoob Javed, M., 2020. Novel Grass Hopper optimization based MPPT of PV systems for complex partial shading conditions. Sol. Energy 198, 499–518. https://doi.org/10.1016/j.solener.2020.01.070. ISSN 0038-092X.

Muniyandi, V., Manimaran, S., Balasubramanian, A.K., 2023. Improving the power output of a partially shaded photovoltaic array through a hybrid magic square configuration with differential evolution-based adaptive P&O MPPT method. J. Sol. Energy Eng. 145 (5), 051001.

Naik, K.A., Raj, R.D.A., Rao, C.V., Babu, T.S., 2022a. Generalized cryptographic image processing approaches using integer-series transformation for solar power optimization under partial shading. Energy Convers. Manag. 272, 116376.

Naik, K.A., Raj, R.D.A., Rao, C.V., Babu, T.S., 2022b. Generalized cryptographic image processing approaches using integer-series transformation for solar power optimization under partial shading. Energy Convers. Manag. 272, 116376.

Nasiruddin, I., Khatoon, S., Jalil, M.F., Bansal, R.C., 2019. Shade diffusion of partial shaded PV array by using odd-even structure. Sol. Energy 181, 519–529.

Nihanth, M.S.S., Ram, J.P., Pillai, D.S., Ghias, A.M., Garg, A., Rajasekar, N., 2019. Enhanced power production in PV arrays using a new skyscraper puzzle based one-time reconfiguration procedure under partial shade conditions (PSCs). Sol. Energy 194, 209–224.

Nihanth, M.S.S., Rajasekar, N., Pillai, D.S., Prasanth Ram, J., 2020. A new array reconfiguration scheme for solar pv systems under partial shading conditions. In: Intelligent Computing Techniques for Smart Energy Systems: Proceedings of ICTSES 2018. Springer, Singapore, pp. 387–396.

Omer, Abdalla, Hegazy, Rezk, Ahmed, Emad M., 2019. Wind driven optimization algorithm based global MPPT for PV system under non-uniform solar irradiance. Sol. Energy 180, 429–444. https://doi.org/10.1016/j.solener.2019.01.056. ISSN 0038-092X.

Raiker, G.A., Loganathan, U., 2021. Current control of boost converter for PV interface with momentum-based perturb and observe MPPT. IEEE Trans. Ind. Appl. 57 (4), 4071–4079.

Raj, R.D.A., Naik, K.A., 2022a. Optimal reconfiguration of PV array based on digital image encryption algorithm: a comprehensive simulation and experimental investigation. Energy Convers. Manag. 261, 115666.

Raj, R.D.A., Naik, K.A., 2022b. Optimal reconfiguration of PV array based on digital image encryption algorithm: a comprehensive simulation and experimental investigation. Energy Convers. Manag. 261, 115666.

Raj, R.D.A., Naik, K.A., 2023a. Priority queue-based switching matrix algorithm for adaptive neuro-fuzzy inference system assisted MPPT controlled PV system. Energy Convers. Manag. 293, 117519.

Raj, R.D.A., Naik, K.A., 2023b. Novel shade dispersion techniques for reconfiguration of partially shaded photovoltaic arrays. Smart Grids and Sustainable Energy 8 (1), 5.

Raj, R.D.A., Naik, K.A., 2023c. A novel scan pattern for reconfiguration of partially shaded photovoltaic arrays for maximum power extraction. Int. J. Circ. Theor. Appl. 51 (2), 668–701.

Raj, R.D.A., Bhattacharjee, S., Biswas, M., 2020. Electrical reconfiguration technique for partially shaded PV arrays with minimal interconnections. In: 2020 International Conference on Power Electronics & IoT Applications in Renewable Energy and its Control (PARC). IEEE, pp. 90–95.

Rani, B.I., Ilango, G.S., Nagamani, C., 2013. Enhanced power generation from PV array under partial shading conditions by shade dispersion using Su Do Ku configuration. IEEE Trans. Sustain. Energy 4 (3), 594–601.

Rao, C.V., et al., 2023. A novel hybrid image processing-based reconfiguration with RBF neural network MPPT approach for improving global maximum power and effective tracking of PV system. Int. J. Circ. Theor. Appl. https://doi.org/10.1002/cta.3629.

Rayappa David Amar Raj, et al., 2023. Priority queue-based switching matrix algorithm for adaptive neuro-fuzzy inference system assisted MPPT controlled PV system. Energy Convers. Manag. 293, 117519.

Reddy, S.S., Yammani, C., 2020. Odd-Even-Prime pattern for PV array to increase power output under partial shading conditions. Energy 213, 118780.

Sahu, H.S., Nayak, S.K., Mishra, S., 2015. Maximizing the power generation of a partially shaded PV array. IEEE journal of emerging and selected topics in power electronics 4 (2), 626–637.

Sajid, Injila, Sarwar, Adil, Tariq, Mohd, Bakhsh, Farhad Ilahi, Ahmad, Shafiq, Mohamed, Adamali Shah Noor, 2023. Archimedes optimization algorithm (AOA)-Based global maximum power point tracking for a photovoltaic system under partial and complex shading conditions. Energy 283, 129169. https://doi.org/10.1016/j.energy.2023.129169. ISSN 0360-5442.

Sharma, N.K., Kumar, S., Kumar, N., 2023. HGSmark: an efficient ECG watermarking scheme using hunger games search and Bayesian regularization BPNN. Biomed. Signal Process Control 83, 104633.

Sing, B., 2004. Kolakoski sequences–an example of aperiodic order. J. Non-Cryst. Solids 334, 100–104.

Subha, R., Himavathi, S., 2018. Active power control of a photovoltaic system without energy storage using neural network-based estimator and modified P&O algorithm. IET Gener., Transm. Distrib. 12 (4), 927–934.

Tatabhatla, V.M.R., Agarwal, A., Kanumuri, T., 2020. A generalized chaotic baker map configuration for reducing the power loss under shading conditions. Electr. Eng. 102, 2227–2244.

Velasco-Quesada, G., Guinjoan-Gispert, F., Piqué-López, R., Román-Lumbreras, M., Conesa-Roca, A., 2009. Electrical PV array reconfiguration strategy for energy extraction improvement in grid-connected PV systems. IEEE Trans. Ind. Electron. 56 (11), 4319–4331.

Venkateswari, R., Rajasekar, N., 2020. Power enhancement of PV system via physical array reconfiguration based Lo Shu technique. Energy Convers. Manag. 215, 112885.

Yang, Bo, Wu, Shaocong, Huang, Jianxiang, Guo, Zhengxun, Wang, Jiarong, Zhang, Zijian, Xie, Rui, Shu, Hongchun, Jiang, Lin, 2023. Salp swarm optimization algorithm based MPPT design for PV-TEG hybrid system under partial shading conditions. Energy Convers. Manag. 292, 117410 https://doi.org/10.1016/j.enconman.2023.117410. ISSN 0196-8904.